



**HAL**  
open science

# Numerical approximations of a lattice Boltzmann scheme with a family of partial differential equations

Bruce M Boghosian, François Dubois, Pierre Lallemand

► **To cite this version:**

Bruce M Boghosian, François Dubois, Pierre Lallemand. Numerical approximations of a lattice Boltzmann scheme with a family of partial differential equations. 2024. hal-04523572v2

**HAL Id: hal-04523572**

**<https://hal.science/hal-04523572v2>**

Preprint submitted on 2 Aug 2024

**HAL** is a multi-disciplinary open access archive for the deposit and dissemination of scientific research documents, whether they are published or not. The documents may come from teaching and research institutions in France or abroad, or from public or private research centers.

L'archive ouverte pluridisciplinaire **HAL**, est destinée au dépôt et à la diffusion de documents scientifiques de niveau recherche, publiés ou non, émanant des établissements d'enseignement et de recherche français ou étrangers, des laboratoires publics ou privés.

# Numerical approximations of a lattice Boltzmann scheme with a family of partial differential equations

Bruce M. Boghosian<sup>ab</sup>, François Dubois<sup>cd</sup> and Pierre Lallemand<sup>e</sup>

<sup>a</sup> *Department of Mathematics, Tufts University, Medford, MA, 02155, USA.*

<sup>b</sup> *present address: American University of Armenia,  
40 Baghramyan Avenue, Yerevan 0019, Armenia.*

<sup>c</sup> *Laboratoire de Mathématiques d'Orsay, Faculté des Sciences d'Orsay,  
Université Paris-Saclay, France.*

<sup>d</sup> *Conservatoire National des Arts et Métiers, LMSSC laboratory, Paris, France.*

<sup>e</sup> *Beijing Computational Science Research Center, Haidian District, Beijing 100094, China.*

02 August 2024 \*

**Keywords:** partial differential equations, asymptotic analysis

**AMS classification:** 76N15, 82C20.

**PACS numbers:** 02.70.Ns, 47.10.+g

## Abstract

In this contribution, we address the numerical solutions of high-order asymptotic equivalent partial differential equations with the results of a lattice Boltzmann scheme for an inhomogeneous advection problem in one spatial dimension. We first derive a family of equivalent partial differential equations at various orders, and we compare the lattice Boltzmann experimental results with a spectral approximation of the differential equations. For an unsteady situation, we show that the initialization scheme at a sufficiently high order of the microscopic moments plays a crucial role to observe an asymptotic error consistent with the order of approximation. For a stationary long-time limit, we observe that the measured asymptotic error converges with a reduced order of precision compared to the one suggested by asymptotic analysis.

---

\* This contribution has been presented at the 19th International Conference for Mesoscopic Methods in Engineering and Science, Mount Qing-Cheng (Chengdu, Sichuan, China) the 25 July 2023 and at Institut Henri Poincaré the 04 October 2023.

## 1) Introduction

The classical framework for numerical simulation starts from partial differential equations. After discretization with some numerical method (finite differences, finite elements, *etc.*), numerical software is developed. Then an approximate solution of the original partial differential equation is computed. A large number of high-quality books exist on this subject. We refer to the works of Oden and Reddy [40], Ferziger and Perić [24], Lucquin and Pironneau [38], among others.

With cellular automata and lattice Boltzmann schemes, this paradigm is reversed. The computing algorithm is the starting point of the study. Then an asymptotic analysis is conducted to derive the underlying continuous equations. The reader can consult, *e.g.*, the books of Rothman and Zaleski [43], Succi [46], Guo and Shu [27], or Krüger *et al.* [34].

Our approach is to derive a physical model from the algorithm. In this work, we adopt the paradigm of multirelaxation lattice Boltzmann schemes [31]. Other variants are possible and there are rational ways to proceed from a partial differential equation system with suitable structure to a kinetic formulation, and hence to a lattice Boltzmann scheme by further discretisation in space and time, *e.g.* by integration along characteristics (He and Luo [28], He *et al.* [30], Dellar [15]). The classical approach for approaching the continuous Boltzmann equation is the Chapman-Enskog method [12]. It has been revisited in Chen and Doolen [13] and Qian and Zhou [42] to take into consideration the discrete aspects of space and time with cellular automata and lattice Boltzmann schemes.

One important remark has to do with the choice of scaling. In this contribution, we suppose acoustic scaling: the ratio between the spatial step and the time step is fixed. Then it is possible to derive asymptotic partial differential equations in terms of a purely numerical parameter, *e.g.* the spatial step to fix the ideas. Taylor expansions allow us to derive equivalent partial differential equations [16, 17]. Dubois *et al.* have established that this Taylor expansion method is equivalent to the Chapman-Enskog approach [19]. This asymptotic expansion is obtained by formal arguments and can be compared to the truncation error of a finite difference scheme. Observe that the relaxation coefficients are supposed fixed when we adopt the acoustic scaling hypothesis.

When an asymptotic partial differential equation is known, it is possible to fit some parameters of the scheme to obtain super convergence. This was done by d’Humières and Ginzburg [33], Augier *et al.* [2], Dubois and Lallemand [20, 21] and Otomo *et al.* [41]. In the present contribution, we fix the relaxation coefficients and consider the spatial step as tending to zero.

An asymptotic expansion is not identical to a convergence result. With the acoustic scaling at second order to fix ideas, the diffusivity is proportional to the spatial step and vanishes as the spatial step tends to zero. Moreover, the truncation error is *a priori* not identical to the mathematical error. Some ad hoc stability and consistency are necessary to establish convergence, as classically established by Lax and Richtmyer in [36]. After the pioneering work of Dellacherie [14], Boghosian *et al.* have established in [8, 9] that the lattice Boltzmann method does not converge for a simple heat equation. The acoustic scaling necessitates

modification of the relaxation coefficients to maintain fixed diffusivity. In consequence, the hypothesis of fixed relaxation coefficients is no longer valid, and the target partial differential equation is not valid for very small spatial steps. Nevertheless, the asymptotic expansion with acoustic scaling is correct. It is simply defining a partial differential equation that mimics the lattice Boltzmann scheme at a specific order of accuracy when the relaxation coefficients are fixed and the spatial step tends to zero.

Our methodology to develop an asymptotic analysis is based on the ABCD method of analysis [18] enforced by the equivalence with the Chapman-Enskog expansion [19]. It allows a fourth-order analysis in a wide class of nonlinear lattice Boltzmann schemes. Thus an important question is the comparison between the simulation with a lattice Boltzmann scheme and reference solutions of the equivalent partial differential equations. The objective of this contribution is to address the numerical solution of high-order equivalent asymptotic partial differential equations with a lattice Boltzmann scheme. We work with an elementary D1Q3 one-dimensional lattice Boltzmann scheme with a prescribed sinusoidal velocity. We treat the reference asymptotic partial differential equations with an approach reminiscent of early kinematic dynamo simulations from the 1980s using pure spectral methods to solve the magnetic induction equation in “ABC” flow (*e.g.* Galloway and Frisch [25]). With this spectral approach we can numerically solve with great precision the family of equivalent partial differential equations at various orders.

As a classical tool of analysis, we use the one-point spectral analysis developed in Lallemand and Luo [35] (see also Simonis *et al.* [45]). We use also Arnoldi iterations [1] for the determination of global modes for an entire mesh, as Verberg and Ladd [47] to compute steady solutions of linear lattice Boltzmann schemes for Stokes flow using a Krylov-space method of Leriche *et al.* [37] for the determination of Stokes eigenmodes in a cubic domain. For many simulations, the initialisation of the lattice Boltzmann state is taken to be an equilibrium. This simple approach has been enriched by first-order initialization initially suggested to our knowledge by Mei *et al.* [39]. Within the framework of Bellotti *et al.* [4], a lattice Boltzmann scheme is revisited as a multistep method for the conserved variables. The equivalent partial differential equations have been established at second-order accuracy with this framework under acoustic scaling [5]. Last but not least, the contribution of Mei *et al.* [39] at first-order accuracy has been revisited by Bellotti [6].

The outline for this work is as follows. In Section 2, we study the reference model: the advection equation in one spatial dimension with a given cosine velocity field. The method of characteristics yields an analytic solution. In Section 3, we present our variant of the D1Q3 lattice Boltzmann scheme, introduced initially by Broadwell [11] in the context of simple discrete-velocity gases. In the lattice Boltzmann framework, dynamics is captured with particles and the relaxation process occurs in the space of moments [31]. They are divided into two families: the conserved moments and the microscopic variables in the denomination proposed by Gatignol [26].

Then, in Section 4 we present the “ABCD” asymptotic analysis [18, 19]. From the precise algebraic expression of a multirelaxation lattice Boltzmann scheme [31, 32], we derive from a formal exponential expression a set of equivalent partial differential equations up to fourth

order accuracy. Here we adapt the underlying algebra first to the case of an inhomogeneous advection problem in one spatial dimension, and we derive a family of equivalent partial differential equations at various orders.

In Section 5, the Fourier series method is adapted to treat in a precise way the case of a cosine advective field. Then the unsteady evolution is presented in Section 6. A first result is relative to a constant velocity and an initial sinusoidal wave. Then we take into account a cosine advection velocity with a sinusoidal or a constant initial condition. We compare the lattice Boltzmann results and a spectral approximation of the differential equations. An interesting phenomenon of lack of convergence is encountered. This motivates the next Section relative to the initialization of microscopic moments. In Section 8, we present our numerical experiments with a detailed asymptotic analysis. Various parameters are considered: the type of problem, with constant or cosine advective velocity, the approximation order of the partial differential equation, the number of mesh points and the initialization process. In Section 9, we study the long-time asymptotics. We observe that the measured asymptotic error is still converging.

This work is the result of conversations in Medford (MA, USA) during summer 2018, and then in Paris in spring 2019. Independent numerical experiments were done during COVID in spring 2020, and complementary work in Beijing in summer 2023.

## 2) Advection with harmonic velocity in one space dimension

We introduce a reference length  $L > 0$ , a final time  $T$  and a reference scale velocity  $\lambda > 0$ . For a given scalar  $U \in \mathbb{R}$  and for  $0 \leq x \leq L$ , we consider the regular periodic velocity field

$$(1) \quad u(x) = \lambda U \cos(kx), \quad k = \frac{2\pi}{L}.$$

The linear inhomogeneous advection equation is the first-order partial differential equation

$$(2) \quad \frac{\partial \rho}{\partial t} + \lambda \frac{\partial}{\partial x} [U \cos(kx) \rho] = 0.$$

We introduce a periodic function  $[0, L] \ni x \mapsto \rho_0(x) \in \mathbb{R}$  as an initial condition

$$(3) \quad \rho(x, 0) = \rho_0(x).$$

Moreover, we suppose periodic boundary conditions throughout this study.

### Proposition 1. Method of characteristics

The differential equation associated with the method of characteristics for the partial differential equation (2) is written

$$(4) \quad \frac{dX}{dt} = \lambda u(X(t)) \equiv \lambda U \cos(kX(t)).$$

With the initial condition  $X(0) = x_0$  with  $0 \leq x_0 \leq L$ , the solution is:

$$(5) \quad \cotg \frac{\pi X}{L} = \frac{\operatorname{th} \frac{\pi t}{T} + \cotg \frac{\pi x_0}{L}}{1 + \operatorname{th} \frac{\pi t}{T} \cotg \frac{\pi x_0}{L}}$$

with  $\lambda U \equiv \frac{L}{T}$ ,  $\operatorname{th} \varphi \equiv \frac{\exp \varphi - \exp(-\varphi)}{\exp \varphi + \exp(-\varphi)}$  and  $\cotg \varphi \equiv \frac{1}{\tan \varphi}$ .

Proof of Proposition 1.

If  $t = 0$ , then  $\cotg \frac{\pi X}{L} = \cotg \frac{\pi x_0}{L}$  and  $\pi \frac{X-x_0}{L}$  is a multiple of  $\pi$ . Then the position  $X = x_0$  is well defined in the interval  $[0, L]$ . Moreover, we have the following calculation:

$$-\frac{1}{\sin^2 \frac{\pi X}{L}} \frac{\pi}{L} \frac{dX}{dt} = \frac{\pi}{T} \frac{(1 - \text{th}^2 \frac{\pi t}{T})(1 - \cotg^2 \frac{\pi x_0}{L})}{(1 + \text{th} \frac{\pi t}{T} \cotg \frac{\pi x_0}{L})^2} = -\frac{\pi}{T} \frac{1}{\sin^2 \frac{\pi X}{L}} \cos \frac{2\pi X}{L}$$

Then  $\frac{dX}{dt} = \frac{L}{T} \cos \frac{2\pi X}{L}$  and the differential equation (4) is satisfied.  $\square$

**Proposition 2. Algebraic solution of the inhomogeneous advection equation**

Given  $x \in [0, L]$  and  $t > 0$ , the solution  $\rho(x, t)$  of the equation (2) satisfying the initial condition (3) is given by the relation

$$\rho(x, t) \cos \left( \frac{2\pi x}{L} \right) = \rho_0(x_0) \cos \left( \frac{2\pi x_0}{L} \right)$$

where  $x_0$  satisfies

$$(6) \quad \cotg \frac{\pi x_0}{L} = \frac{\cotg \frac{\pi x}{L} - \text{th} \frac{\pi t}{T}}{1 - \text{th} \frac{\pi t}{T} \cotg \frac{\pi x_0}{L}}.$$

Proof of Proposition 2.

We search for the foot  $x_0$  of the characteristic  $t \mapsto X(t)$  (4) such that  $X(0) = x_0$  and  $X(t) = x$ . The characteristic passing through point  $x$  at time  $t$  then satisfies the two relations  $X(0) = x_0$  and  $X(t) = x$ . First, we deduce from the partial differential equation (2) that the product  $\rho(x, t) \cos \left( \frac{2\pi x}{L} \right)$  remains constant. Second, from the relation (5), we deduce the relation (6) for defining  $x_0$ .  $\square$

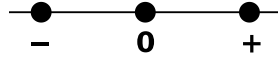


Figure 1: D1Q3 lattice Boltzmann scheme

### 3) D1Q3 lattice Boltzmann scheme

The scale velocity  $\lambda > 0$  is now equal to the ratio between the spatial step  $\Delta x$  and the time step  $\Delta t$ :

$$\lambda = \frac{\Delta x}{\Delta t}.$$

From the particle distribution  $f \equiv (f_+, f_0, f_-)^t$  presented in Figure 1, we construct a single conserved moment  $W$  denoted “density” in the following:  $\rho = f_+ + f_0 + f_-$ . We have also two non-conserved microscopic moments  $Y = (J, e)^t$  with the “momentum”  $J = \lambda f_+ - \lambda f_-$  and the “energy”  $e = \lambda^2 (f_+ - 2f_0 + f_-)$ . Then the family of moments  $m \equiv (W, Y)$  is linked to the particles  $f$  with the d’Humières [31] matrix  $M$ :  $m \equiv M f$ , with

$$M = \begin{pmatrix} 1 & 1 & 1 \\ \lambda & 0 & -\lambda \\ \lambda^2 & -2\lambda^2 & \lambda^2 \end{pmatrix}.$$

For an inhomogeneous linear equilibrium  $Y^{\text{eq}} = \Phi(W) = E(x)W$ , the equilibrium matrix  $E(x)$  is a function of space. In the case of an advective field  $u(x)$  proposed in the relation (1), we have

$$E(x) = \begin{pmatrix} \lambda U \cos(kx) \\ \lambda^2 \alpha \end{pmatrix}$$

with a coefficient  $\alpha = -1$  in our numerical experiments.

The relaxation  $Y \mapsto Y^*$  of the nonconserved moments  $Y$  is classical:

$$\begin{cases} J^* = J + s(J^{\text{eq}} - J) = (1 - s)J + s\lambda U \cos(kx)\rho \\ e^* = e + s'(e^{\text{eq}} - e) = (1 - s')e + s'\lambda^2 \alpha \rho \end{cases}$$

and we have chosen  $s = 1.5$ ,  $s' = 1.2$  in our reference numerical experiments. Observe that the parameters  $U$ ,  $\alpha$ ,  $s$  and  $s'$  are without dimension. We set finally  $m^* = (\rho, J^*, e^*)^t$ .

The collision step is defined according to  $f^* = M^{-1}m^*$ , and the exact propagation of particles along the characteristic directions  $\lambda, 0, -\lambda$  of the D1Q3 scheme:

$$\begin{cases} f_+(x, t + \Delta t) = f_+(x - \Delta x, t) \\ f_0(x, t + \Delta t) = f_0(x, t) \\ f_-(x, t + \Delta t) = f_-(x + \Delta x, t) \end{cases}$$

is well known (see *e.g.* [31]). The solution of this lattice Boltzmann scheme can be approached by the first order equivalent partial differential equation

$$\frac{\partial \rho}{\partial t} + \lambda \frac{\partial}{\partial x} [U \cos(kx) \rho] = O(\Delta x).$$

Therefore, it is natural to compare the numerical solution of the D1Q3 lattice Boltzmann scheme with the exact solution of the inhomogeneous advection equation (2). We have done this work in a first numerical experiment, and the results are displayed in Figure 2.

During the first time steps (see the results for  $T = 01$  and  $T = 10$ ), the two results agree with good precision. But we observe that the solution of the advection equation (2) is unsteady, whereas the lattice Boltzmann scheme rapidly converges towards a stationary solution. Then the approximation of the D1Q3 scheme by the first-order partial differential equation is not sufficient. We adapt a complementary analysis in the next section.

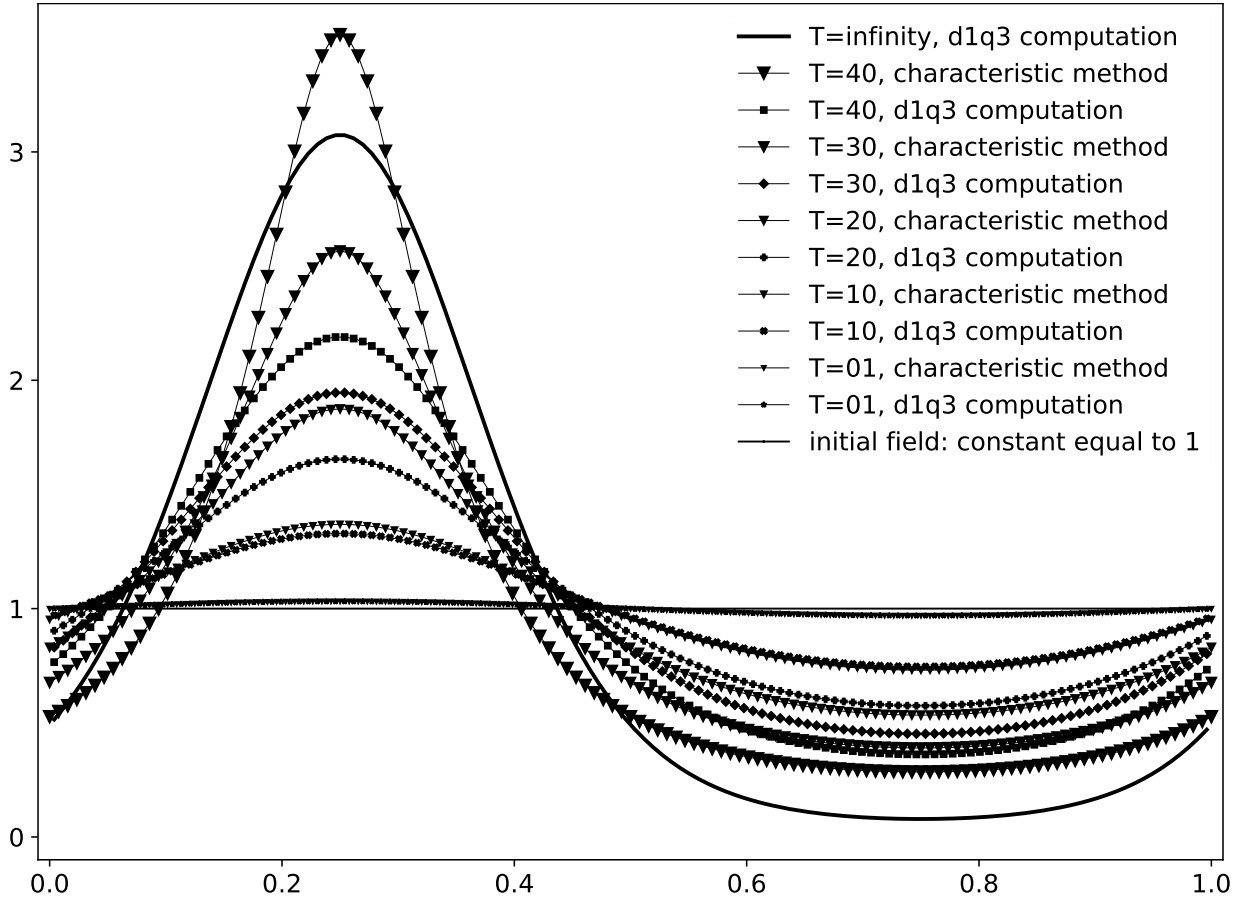


Figure 2: Evolution for an advective velocity (1) with  $U = 0.005$  and  $N = 128$  mesh points. We observe that with the cosine advection velocity, the numerical solution has no symmetry. As time progresses, we observe that the characteristic method becomes less and less precise.

#### 4) ABCD asymptotics in the isotropic linear case

In this section, we revisit the ‘‘Berlin algorithm’’ introduced in [3] for the linear analysis of lattice Boltzmann schemes. First recall that one time step is comprised of two stages:

(i) nonlinear relaxation

$$m \mapsto m^* \equiv \begin{pmatrix} W^* \\ Y^* \end{pmatrix}, \quad W^* = W, \quad Y^* = Y + S(\Phi(W) - Y)$$

with a diagonal relaxation matrix  $S$ . Observe that with our definition, the relaxation matrix  $S$  only concerns the nonconserved microscopic moments. In consequence, for the D1Q3 scheme, we have  $S = \text{diag}(s, s')$ .

(ii) linear advection

$$m^* \mapsto f(t + \Delta t) : f^* = M^{-1} m^*, \quad f_j(x, t + \Delta t) = f_j^*(x - v_j \Delta t, t).$$

The operator of advection of moments  $\Lambda$  is defined from the diagonal advection operator  $\sum_{\alpha} v^{\alpha} \partial_{\alpha}$  according to [18]

$$\Lambda \equiv M \text{diag} \left( \sum_{1 \leq \alpha \leq d} v^{\alpha} \partial_{\alpha} \right) M^{-1}$$



with  $d$  the spatial dimension. This is nothing more than the advection operator in the basis of moments. Following a remark proposed in [18], we have an exact exponential expression of the lattice Boltzmann scheme

$$m(x, t + \Delta t) = \exp(-\Delta t \Lambda) m^*(x, t).$$

We can expand this relation up to fourth order to obtain

$$m(x, t + \Delta t) = \left[ \mathbb{I} - \Delta t \Lambda + \frac{\Delta t^2}{2} \Lambda^2 - \frac{\Delta t^3}{6} \Lambda^3 + \frac{\Delta t^4}{24} \Lambda^4 + \mathcal{O}(\Delta t^5) \right] m^*(x, t).$$

The equivalent partial differential equations of the scheme are found from the asymptotic expansion (see *e.g.* [19])

$$\partial_t = \partial_{t_1} + \Delta t \partial_{t_2} + \Delta t^2 \partial_{t_3} + \Delta t^3 \partial_{t_4} + \mathcal{O}(\Delta t^3).$$

Consider now the ‘‘ABCD’’ block decomposition (see [19]) of the momentum-velocity operator that is obtained for the D1Q3 lattice Boltzmann scheme:

$$\Lambda \equiv \begin{pmatrix} A & B \\ C & D \end{pmatrix} = \left( \begin{array}{c|cc} 0 & \partial_x & 0 \\ \frac{2}{3} \lambda^2 \partial_x & 0 & \partial_x \\ 0 & \lambda^2 \partial_x & 0 \end{array} \right).$$

Asymptotic analysis is carried out to second order. It uses only a small set of mathematical expressions:

$$(7) \quad \begin{cases} \partial_{t_1} W + \Gamma_1 = 0 \\ \partial_{t_2} W + \Gamma_2 = 0 \\ \Gamma_1 = A W + B \Phi(W) \\ Y = \Phi(W) + \Delta t S^{-1} \Psi_1 + \mathcal{O}(\Delta t^2) \\ \Psi_1 = d\Phi(W) \cdot \Gamma_1 - (C W + D \Phi(W)) \\ \Sigma \equiv S^{-1} - \frac{1}{2} \mathbb{I} \\ \Gamma_2 = B \Sigma \Psi_1. \end{cases}$$

The application to the Navier Stokes equations can be found in [23]. For the fourth-order analysis, these relations are enriched in the following way [18, 19]. We first extend the asymptotic expansion for the microscopic moments

$$(8) \quad Y = \Phi(W) + S^{-1} (\Delta t \Psi_1(W) + \Delta t^2 \Psi_2(W) + \Delta t^3 \Psi_3(W)) + \mathcal{O}(\Delta t^4).$$

We observe that the operators  $\Psi_j$  are *a priori* nonlinear operators of order  $j$ . The partial differential equation for the conserved moments takes the form

$$\partial_{t_1} W + \Gamma_1 = 0, \quad \partial_{t_2} W + \Gamma_2 = 0, \quad \partial_{t_3} W + \Gamma_3 = 0, \quad \partial_{t_4} W + \Gamma_4 = 0.$$

The differential operators at third order are obtained by nontrivial algebra [18, 19]:

$$(9) \quad \begin{cases} \Psi_2(W) = \Sigma d\Psi_1(W) \cdot \Gamma_1(W) + d\Phi(W) \cdot \Gamma_2(W) - D \Sigma \Psi_1(W) \\ \Gamma_3(W) = B \Sigma \Psi_2(W) + \frac{1}{12} B_2 \Psi_1(W) - \frac{1}{6} B d\Psi_1(W) \cdot \Gamma_1(W) \end{cases}$$

and it is also the case for the fourth-order terms:

$$(10) \quad \begin{cases} \Psi_3(W) = \Sigma d\Psi_1(W) \cdot \Gamma_2(W) + d\Phi(W) \cdot \Gamma_3(W) - D \Sigma \Psi_2(W) + \Sigma d\Psi_2(W) \cdot \Gamma_1(W) \\ \quad + \frac{1}{6} D d\Psi_1(W) \cdot \Gamma_1(W) - \frac{1}{12} D_2 \Psi_1(W) - \frac{1}{12} d(d\Psi_1(W) \cdot \Gamma_1) \cdot \Gamma_1(W) \\ \Gamma_4(W) = B \Sigma \Psi_3(W) + \frac{1}{4} B_2 \Psi_2(W) + \frac{1}{6} B D_2 \Sigma \Psi_1(W) - \frac{1}{6} A B \Psi_2(W) \\ \quad - \frac{1}{6} B (d(d\Phi \cdot \Gamma_1) \cdot \Gamma_2(W) - \frac{1}{6} B d(d\Phi \cdot \Gamma_2) \cdot \Gamma_1(W)) \\ \quad - \frac{1}{6} B \Sigma d(d\Psi_1(W) \cdot \Gamma_1) \cdot \Gamma_1(W), \end{cases}$$

with

$$\begin{pmatrix} A_2 & B_2 \\ C_2 & D_2 \end{pmatrix} \equiv \begin{pmatrix} A & B \\ C & D \end{pmatrix} \begin{pmatrix} A & B \\ C & D \end{pmatrix} = \begin{pmatrix} A^2 + BC & AB + BD \\ CA + DC & CB + D^2 \end{pmatrix}.$$

In one spatial dimension, the previous A, B, C, D differential operators factorize into algebraic expressions multiplying  $x$ -derivatives:

$$(11) \quad A \equiv \bar{A} \partial_x, \quad B \equiv \bar{B} \partial_x, \quad C \equiv \bar{C} \partial_x, \quad D \equiv \bar{D} \partial_x.$$

In this context of one spatial dimension, we introduce an inhomogeneous equilibrium:

$$(12) \quad \Phi(W) \equiv E(x) W.$$

Then we can define a new inhomogeneous differential operator  $\delta$  with

$$(13) \quad \delta W \equiv \partial_x(\Phi(W)) = \partial_x(E(x) W).$$

We have  $\delta = \frac{\partial E}{\partial x} I + E(x) \partial_x$ . Then we observe that the commutator  $[\partial_x, \delta] \equiv \partial_x \delta - \delta \partial_x$  is not equal to zero:  $[\partial_x, \delta] \varphi = \partial_x \partial_x(E(x) \varphi) - \partial_x(E(x) \partial_x \varphi) = \partial_x((\partial_x E) \varphi)$ .

### Proposition 3. Differential operators for linear nonuniform advection

In the previous context of a linear inhomogeneous scheme, the differential operators  $\Gamma_1, \Psi_1, \Gamma_2, \Psi_2, \Gamma_3, \Psi_3$  and  $\Gamma_4$ , defined at the relations (7)(9)(10), take the form

$$\Gamma_j \equiv \alpha_j W, \quad \Psi_j \equiv \beta_j W$$

with the following algebraic relations

$$(14) \quad \begin{cases} \alpha_1 = \bar{A} \partial_x + \bar{B} \delta \\ \beta_1 = E \alpha_1 - (\bar{C} \partial_x + \bar{D} \delta) \\ \alpha_2 = \bar{B} \Sigma \partial_x \beta_1 \\ \beta_2 = \Sigma \beta_1 \alpha_1 + E \alpha_2 - \bar{D} \Sigma \partial_x \beta_1 \\ \alpha_3 = \bar{B} \Sigma \partial_x \beta_2 + \frac{1}{12} \bar{B}_2 \partial_x^2 \beta_1 - \frac{1}{6} \bar{B} \partial_x \beta_1 \alpha_1 \\ \beta_3 = \Sigma \beta_1 \alpha_2 + E \alpha_3 - \bar{D} \Sigma \partial_x \beta_2 + \Sigma \beta_2 \alpha_1 + \frac{1}{6} \bar{D} \partial_x \beta_1 \alpha_1 - \frac{1}{12} \beta_1 \alpha_1^2 - \frac{1}{12} \bar{D}_2 \partial_x^2 \beta_1 \\ \alpha_4 = \bar{B} \Sigma \partial_x \beta_3 + \frac{1}{4} \bar{B}_2 \partial_x^2 \beta_2 + \frac{1}{6} \bar{B} \bar{D}_2 \Sigma \partial_x^3 \beta_1 - \frac{1}{6} \bar{A} \bar{B} \partial_x^2 \beta_2 \\ \quad - \frac{1}{6} \bar{B} \delta \alpha_1 \alpha_2 - \frac{1}{6} \bar{B} \delta \alpha_2 \alpha_1 - \frac{1}{6} \bar{B} \Sigma \partial_x \beta_1 \alpha_1^2. \end{cases}$$

The proof of this proposition is a tedious algebraic calculation. It is presented in Annex A.

We consider in this contribution the case of the D1Q3 scheme with one conservation law with a cosine velocity field  $u(x) \equiv \lambda U \cos(kx)$  introduced in (1). Then the differential operator  $\delta$  proposed in (13) takes the form

$$\delta \varphi = \partial_x(E(x) \varphi) = \partial_x \begin{pmatrix} \lambda U \cos(kx) \varphi \\ \lambda^2 \alpha \varphi \end{pmatrix} = \partial_x \begin{pmatrix} u \varphi \\ \lambda^2 \alpha \varphi \end{pmatrix}.$$

With the notation

$$(15) \quad \partial_u \varphi \equiv U \partial_x(\cos(kx) \varphi)$$

if the velocity field is a cosine (*c.f.* (1)) and

$$\partial_u \varphi \equiv U \partial_x \varphi$$

when the velocity field is constant, we have simply

$$(16) \quad \delta = \begin{pmatrix} \lambda \partial_u \\ \lambda^2 \alpha \partial_x \end{pmatrix}.$$

We observe that the differential operators  $\partial_x$  and  $\partial_u$  do not commute:

$$[\partial_x, \partial_u] \varphi = \partial_x(-kU \sin(kx) \varphi).$$

**Proposition 4. D1Q3 differential operators for linear nonuniform advection**

The linear differential operators explicated in (14) admit the following expressions in terms of the operators  $\partial_x$  and  $\partial_u$ . We have for the two first orders

$$(17) \quad \alpha_1 = \lambda \partial_u, \quad \beta_1 = \lambda^2 \left( \frac{u}{\lambda} \partial_u - \frac{\alpha+2}{3} \partial_x \right)$$

$$(18) \quad \begin{cases} \alpha_2 = \lambda^2 \sigma \left( \partial_u^2 - \frac{\alpha+2}{3} \partial_x^2 \right) \\ \beta_2 = \lambda^3 \left( 2\sigma \frac{u}{\lambda} \partial_u^2 - \left( \frac{\alpha+2}{3} \sigma + \frac{\alpha-1}{3} \sigma' \right) \partial_x \partial_u - \frac{\alpha+2}{3} \sigma \frac{u}{\lambda} \partial_x^2 \right) \\ \quad \lambda(\alpha-1) \left( (\sigma + \sigma') \partial_u^2 - \frac{\alpha+2}{3} \sigma \partial_x^2 \right) \end{cases},$$

with the Hénon coefficients [29]  $\sigma$  and  $\sigma'$  defined according to

$$\sigma = \frac{1}{s} - \frac{1}{2}, \quad \sigma' = \frac{1}{s'} - \frac{1}{2}.$$

At third order, the formulae are more complicated. We have

$$(19) \quad \alpha_3 = \lambda^3 \left[ \left( 2\sigma^2 - \frac{1}{6} \right) \partial_u^3 + \left( \frac{\alpha+2}{3} \left( \frac{1}{6} - \sigma^2 \right) + \frac{\alpha-1}{3} \left( \frac{1}{12} - \sigma\sigma' \right) \right) \partial_x^2 \partial_u - \frac{\alpha+2}{3} \sigma^2 \partial_u \partial_x^2 \right]$$

and

$$\beta_3 \equiv \begin{pmatrix} \lambda^4 \beta_{3J} \\ \lambda^5 \beta_{3e} \end{pmatrix},$$

with

$$(20) \quad \begin{cases} \beta_{3J} = \frac{\alpha+2}{9} \left[ - (1-\alpha) \sigma \sigma' + \left( (\alpha+2) \sigma^2 + \frac{1}{4} \right) \right] \partial_x^3 \\ \quad + U \left[ - 2 \frac{\alpha+2}{3} \sigma^2 + \frac{1-\alpha}{3} \sigma \sigma' + \frac{1+\alpha}{12} \right] \partial_x^2 \partial_u - 2U \frac{\alpha+2}{3} \sigma^2 \partial_u \partial_x^2 \\ \quad + \left[ - 2 \frac{\alpha+2}{3} \sigma^2 + \frac{1-\alpha}{3} (2\sigma\sigma' + \sigma'^2 - \frac{1}{4}) \right] \partial_x \partial_u^2 + \left( 5\sigma^2 - \frac{1}{4} \right) U \partial_u^3 \\ \beta_{3e} = \frac{1-\alpha}{3} \left[ (\alpha+2) \sigma^2 + (1+2\alpha) \sigma \sigma' - \frac{1+\alpha}{4} \right] \partial_x^2 \partial_u + (1-\alpha) \frac{\alpha+2}{3} \sigma (\sigma + \sigma') \partial_u \partial_x^2 \\ \quad - (1-\alpha) \left( 2\sigma^2 + 2\sigma\sigma' + \sigma'^2 - \frac{1}{4} \right) \partial_u^3. \end{cases}$$

At fourth order, we have

$$(21) \quad \begin{cases} \alpha_4 = \lambda^4 \left[ \frac{\alpha+2}{9} \left( (\alpha+2) \sigma^3 - (1-\alpha) \sigma^2 \sigma' - \frac{\alpha}{4} \sigma \right) \partial_x^4 \right. \\ \quad + \left[ - 2 \frac{\alpha+2}{3} \sigma^3 + \frac{1-\alpha}{3} (2\sigma^2 \sigma' + \sigma \sigma'^2 - \frac{1}{4} \sigma') + \frac{1+2\alpha}{9} \sigma \right] \partial_x^2 \partial_u^2 \\ \quad + \left[ - 2 \frac{\alpha+2}{3} \sigma^3 + \frac{1-\alpha}{3} \sigma^2 \sigma' + \frac{7+5\alpha}{36} \sigma \right] \partial_u \partial_x^2 \partial_u \\ \quad \left. + \frac{\alpha+2}{3} \sigma \left( - 2\sigma + \frac{1}{6} \right) \partial_u^2 \partial_x^2 + \sigma \left( 5\sigma^2 - \frac{3}{4} \right) \partial_u^4 \right]. \end{cases}$$

The proof of Proposition 4 is detailed in Annex B.

When the velocity field has a constant value  $u(x) \equiv \lambda U$ , super-convergence can be obtained with an appropriate choice of relaxation coefficients, called “magic” in [33]. Because magic is not science, we prefer the denomination of “quartic parameters” [21] to achieve fourth-order accuracy, or “cubic parameter” in the present case to obtain a third-order precision.

When the advection velocity field has a constant value, we have  $\partial_u \equiv U \partial_x$  and the coefficient  $\alpha_3$  initially given according to (19) takes now the value

$$(22) \quad \alpha_3 = \frac{\lambda^3 U}{12} \left[ - 2(1 - 12\sigma^2) U^2 + 4(1-\alpha) \sigma \sigma' + 1 + \alpha - 8(2+\alpha) \sigma^2 \right] \partial_x^3.$$

Then for a fixed set of values for  $U$ ,  $\alpha$  and  $\sigma$ , the cubic parameter  $\sigma'_c$  is defined by forcing to zero the value of  $\alpha_3$  in the relation (22):

$$(23) \quad \sigma'_c = \frac{2(1 - 12\sigma^2)U^2 + 8(2 + \alpha)\sigma^2 - (1 + \alpha)}{4(1 - \alpha)\sigma}.$$

In the following, we first experiment with the D1Q3 lattice Boltzmann scheme with constant velocity, possibly with cubic parameters. Then we consider a cosine advection velocity. We detail in the next section the Fourier methodology developed to solve the various equivalent partial differential equations with very good precision.

## 5) Interlaced Fourier series

We compare the numerical simulation done with the D1Q3 lattice Boltzmann scheme with the solution of the equivalent partial differential equations up to fourth-order accuracy. This hierarchy of equations can be written

$$(24) \quad \frac{\partial \rho}{\partial t} + \sum_{j=1}^{\ell} \Delta t^{j-1} \alpha_j \rho = 0.$$

They are of order  $\ell$  for  $1 \leq \ell \leq 4$ . We recall that we have the following structure

$$\begin{cases} \Delta t^0 \alpha_1 = \lambda \partial_u \\ \Delta t^1 \alpha_2 = -\mu \partial_x^2 + \mu_u \partial_u^2 \\ \Delta t^2 \alpha_3 = \xi_u \partial_u^3 + \xi_{xu} \partial_x^2 \partial_u + \xi_{ux} \partial_u \partial_x^2 \\ \Delta t^3 \alpha_4 = \zeta_{u4} \partial_u^4 + \zeta_{xxuu} \partial_x^2 \partial_u^2 + \zeta_{uxxu} \partial_u \partial_x^2 \partial_u + \zeta_{uuxx} \partial_u^2 \partial_x^2 + \zeta_{x4} \partial_x^4. \end{cases}$$

The coefficients  $\mu$ ,  $\mu_u$ ,  $\xi_u$ ,  $\xi_{xu}$ ,  $\xi_{ux}$ ,  $\zeta_{u4}$ ,  $\zeta_{xxuu}$ ,  $\zeta_{uxxu}$ ,  $\zeta_{uuxx}$  and  $\zeta_{x4}$  are easy to explicate from the relations (17)(18)(19)(21):

$$\begin{cases} \mu = \frac{\alpha+2}{3} \lambda^2 \sigma, \quad \mu_u = \lambda^2 \sigma, \\ \xi_u = \lambda^3 \left( 2\sigma^2 - \frac{1}{6} \right), \quad \xi_{xu} = \lambda^3 \left( \frac{\alpha+2}{3} \left( \frac{1}{6} - \sigma^2 \right) + \frac{\alpha-1}{3} \left( \frac{1}{12} - \sigma \sigma' \right) \right), \quad \xi_{ux} = -\lambda^3 \frac{\alpha+2}{3} \sigma^2 \\ \zeta_{u4} = \lambda^4 \sigma \left( 5\sigma^2 - \frac{3}{4} \right), \quad \zeta_{xxuu} = \lambda^4 \left[ -2 \frac{\alpha+2}{3} \sigma^3 + \frac{1-\alpha}{3} (2\sigma^2 \sigma' + \sigma \sigma'^2 - \frac{1}{4} \sigma') + \frac{1+2\alpha}{9} \sigma \right] \\ \zeta_{uxxu} = \lambda^4 \left[ -2 \frac{\alpha+2}{3} \sigma^3 + \frac{1-\alpha}{3} \sigma^2 \sigma' + \frac{7+5\alpha}{36} \sigma \right], \quad \zeta_{uuxx} = \lambda^4 \frac{\alpha+2}{3} \sigma \left( -2\sigma + \frac{1}{6} \right) \\ \zeta_{x4} = \lambda^4 \left[ \frac{\alpha+2}{9} ((\alpha+2)\sigma^3 - (1-\alpha)\sigma^2 \sigma' - \frac{\alpha}{4} \sigma) \right]. \end{cases}$$

We use a spectral method to capture an approximation of a partial differential equation of the family (24). In the case of an advective field given in (1), we introduce the two discrete spaces  $S_i$  and  $S_p$  defined as follows. The space of odd sine and even cosine is called  $S_i$ :

$$S_i \ni \rho = \sum_{j \geq 0} a_{2j+1} \sin((2j+1)kx) + \sum_{j \geq 0} a_{2j+2} \cos((2j+2)kx)$$

and the space of even sine and odd cosine is denoted by  $S_p$ :

$$S_p \ni \rho = \sum_{j \geq 0} b_{2j+1} \cos((2j+1)kx) + \sum_{j \geq 0} b_{2j+2} \sin((2j+2)kx).$$

The derivation operator breaks down into two parts:

$$\begin{cases} \partial_x^{ip} : S_i \longrightarrow S_p \\ \partial_x^{pi} : S_p \longrightarrow S_i. \end{cases}$$

Relatively to the basis  $(\sin kx, \cos 2kx, \sin 3kx, \cos 4kx, \dots)$  of  $S_i$  and to the basis  $(\cos kx, \sin 2kx, \cos 3kx, \sin 4kx, \dots)$  of  $S_p$ , the operators  $\partial_x^{ip}$  and  $\partial_x^{pi}$  can be represented by the following matrices

$$\begin{cases} \Delta_x^{ip} = \text{diag}(k, -2k, 3k, -4k, \dots) \\ \Delta_x^{pi} = \text{diag}(-k, 2k, -3k, 4k, \dots) = -\Delta_x^{ip}. \end{cases}$$

The second order operator  $\partial_x^2 = \partial_x^{pi} \circ \partial_x^{ip}$  operates inside the space  $S_i$  and is represented by the matrix

$$\Delta_x^{pi} \Delta_x^{ip} = -\text{diag}(k^2, 4k^2, 9k^2, 16k^2, \dots).$$

We introduce also the operator  $m_u$  of multiplication by  $u \equiv U \cos(kx)$ . It operates from  $S_i$  and takes its values in  $S_p$ . Then  $\partial_u = \partial_x \circ m_u$  operates inside the space  $S_i$ . More precisely, we have, without forgetting the constant component  $a_0$ :

$$\begin{aligned} m_u \rho &= U \cos(kx) \left[ a_0 + \sum_{j \geq 0} a_{2j+1} \sin((2j+1)kx) + \sum_{j \geq 0} a_{2j+2} \cos((2j+2)kx) \right] \\ &= (a_0 + \frac{1}{2} a_2) U \cos(kx) + \frac{U}{2} \sum_{j \geq 0} (a_{2j+1} + a_{2j+3}) \sin((2j+2)kx) \\ &\quad + \frac{U}{2} \sum_{j \geq 1} (a_{2j} + a_{2j+2}) \cos((2j+1)kx). \end{aligned}$$

The matrix

$$M_u \equiv \frac{U}{2} \begin{pmatrix} 0 & 1 & 0 & 0 \\ 1 & 0 & 1 & 0 \\ 0 & 1 & 0 & \ddots \\ 0 & 0 & \ddots & \ddots \end{pmatrix}$$

is a natural implementation of the operator  $m_u$  of multiplication by the velocity  $u$  for  $\rho \in S_i$ . Then the differential operator  $\partial_u \equiv \partial_x m_u$  in the space  $S_i$  after truncation is represented by the matrix  $\Delta_x^{pi} M_u$ .

We have used two discretizations with 30 or 60 Fourier modes. Observe that when  $U = 0.05$ , the results are correct with 30 Fourier modes for 64 and 128 mesh points. But with 256 and 512 mesh points, oscillations appear in the numerical results. This is the sign of a under-resolved simulation. We have changed the number of Fourier modes and used 60 modes for 256 and 512 mesh points. We tested the representation of the solution of the D1Q3 scheme with a Fourier series. We have observed a residual in  $\ell^\infty$  norm of  $1.79 \times 10^{-14}$  and  $6.06 \times 10^{-11}$ . This precision is sufficient for our simulations.

After these algebraic operations, the partial differential equation (24) can be seen as an infinite system of ordinary differential equations

$$(25) \quad \frac{\partial \rho}{\partial t} + A \rho = 0$$

with an operator  $A$  given at fourth order by the relation

$$(26) \quad \left\{ \begin{aligned} A &= \lambda \partial_x m_u - \mu \partial_x^2 + \mu_u \partial_x m_u \partial_x m_u \\ &\quad + (\xi_u \partial_x m_u \partial_x m_u \partial_x m_u + \xi_{xu} \partial_x^3 m_u + \xi_{ux} \partial_x m_u \partial_x^2) \\ &\quad + (\zeta_{u4} \partial_x m_u \partial_x m_u \partial_x m_u \partial_x m_u + \zeta_{xxuu} \partial_x^3 m_u \partial_x m_u + \zeta_{uxxu} \partial_x m_u \partial_x^3 m_u \\ &\quad + \zeta_{uuxx} \partial_x m_u \partial_x m_u \partial_x^2 + \zeta_{x4} \partial_x^4). \end{aligned} \right.$$

We observe that the matrix  $A$  is constant. Then after discretization with  $N$  modes, it becomes a constant matrix  $\tilde{A}_N$ . The system (25) is replaced by a system of a finite number of ordinary differential equations

$$(27) \quad \frac{\partial \rho}{\partial t} + \tilde{A}_N \rho = 0.$$

Due to the fact that the matrix  $\tilde{A}_N$  is fixed, the solution of (27) is approached in this contribution for small values of time ( $t$  is replaced by the time step  $\Delta t$  for the numerical integration) by a Taylor expansion at order 5 from the initial condition  $\rho_0$ , an expansion consistent with a spatial precision of order at most 4:

$$\rho(t) = \exp(-t \tilde{A}_N) \rho_0 \simeq \left[ \mathbb{I} - t \tilde{A}_N + \frac{t^2}{2} \tilde{A}_N^2 - \frac{t^3}{6} \tilde{A}_N^3 + \frac{t^4}{24} \tilde{A}_N^4 - \frac{t^5}{120} \tilde{A}_N^5 \right] \rho_0.$$

In an initial series of numerical experiments, we have put in evidence approximations of the stationary solution of a lattice Boltzmann scheme forced with a cosine velocity field.

## 6) Unsteady evolution

We now compare the D1Q3 lattice Boltzmann scheme up to time  $T = 1$  with the Fourier approximations of the various equivalent partial differential equations at various orders

$$\frac{\partial \rho}{\partial t} + A_j \rho = 0, \quad 1 \leq j \leq 4.$$

Observe that  $A_j$  is a continuous partial differential operator whereas  $\tilde{A}_N$  in the previous section is a discretization with  $N$  degrees of freedom. We use a different notation to avoid ambiguity between the order of approximation and the order of discretization. We have at order 1:

$$A_1 = \lambda \partial_x m_u,$$

at order 2:

$$A_2 = A_1 - \mu \partial_x^2 + \mu_u \partial_x m_u \partial_x m_u,$$

at order 3:

$$A_3 = A_2 + (\xi_u \partial_x m_u \partial_x m_u \partial_x m_u + \xi_{xu} \partial_x^3 m_u + \xi_{ux} \partial_x m_u \partial_x^2),$$

and at order 4:

$$\left\{ \begin{array}{l} A_4 = A_3 + (\zeta_{u4} \partial_x m_u \partial_x m_u \partial_x m_u \partial_x m_u + \zeta_{xxuu} \partial_x^3 m_u \partial_x m_u \\ \quad + \zeta_{uxxu} \partial_x m_u \partial_x^3 m_u + \zeta_{uuxx} \partial_x m_u \partial_x m_u \partial_x^2 + \zeta_{x4} \partial_x^4). \end{array} \right.$$

We have chosen the following parameters

$$U = 0.005, \quad \alpha = -1, \quad \sigma = 0.01 \quad [s = 1.960784313725], \quad s' = 1.2$$

with  $\sigma \equiv \frac{1}{s} - \frac{1}{2}$ . The detailed results are presented in a preliminary edition of this work [10].

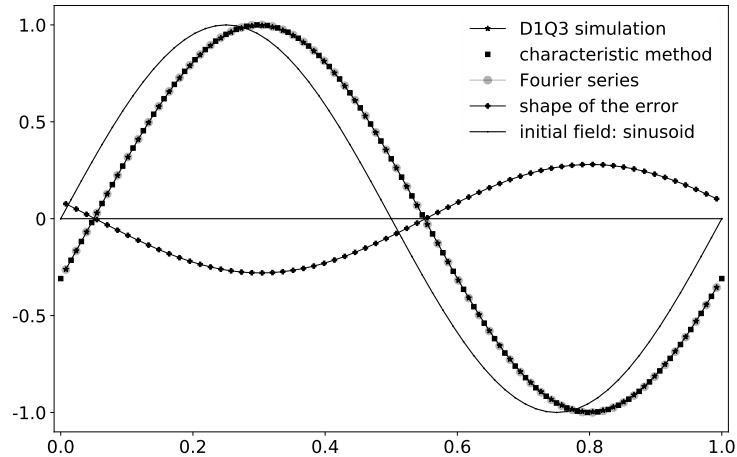


Figure 3: Unsteady evolution, constant advection field [ $U = 0.05$ ], 64 mesh points, sinusoidal initial condition.

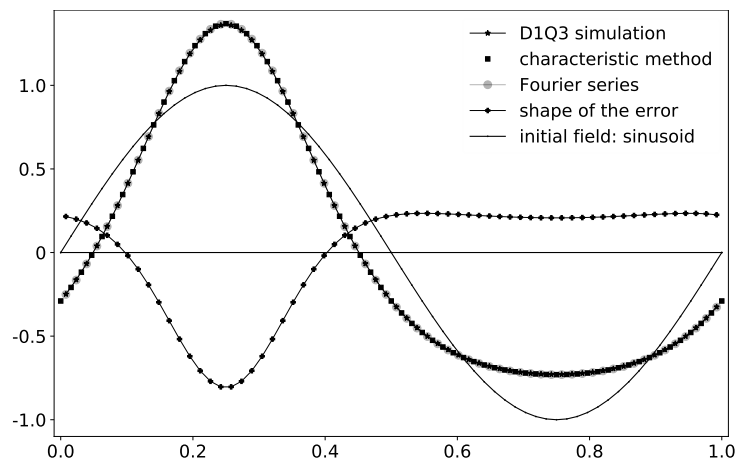


Figure 4: Unsteady evolution, sinusoidal advection field [ $U = 0.05$ ], 64 mesh points, sinusoidal initial condition.

In Figure 3, we consider a constant velocity field with a sinusoidal initial condition. In Figure 4, a cosine velocity field with a sinusoidal initial condition is studied. These figures show that the approximation of the lattice Boltzmann scheme with the equivalent partial differential equations is globally correct. Then we refine the mesh up to  $N = 1024$  points. The results are presented in Figure 5. They are not completely satisfactory.

In order to overcome the moderate speed of convergence for an unsteady evolution, we focus in the next section on the way the lattice Boltzmann scheme is initialized.

## 7) Initialization of microscopic moments

In the previous section, we have taken the non-conserved moments at time  $t = 0$  equal to the value at equilibrium:

$$(28) \quad Y_0(t = 0) = \Phi(\rho_0).$$

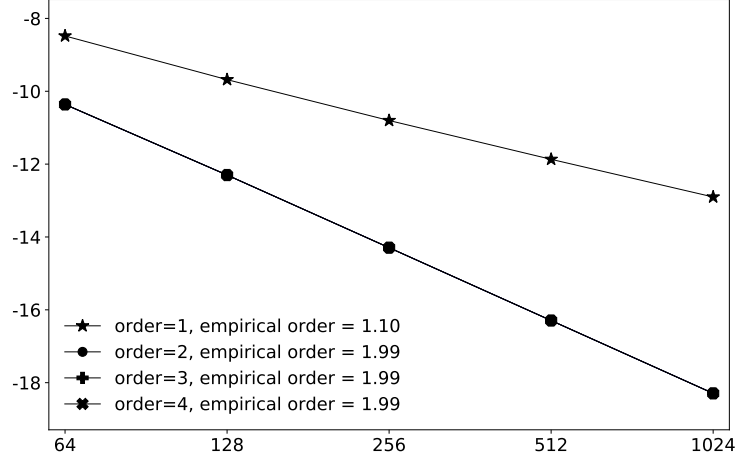


Figure 5: Errors measured with the maximum norm between the D1Q3 lattice Boltzmann scheme and various equivalent partial differential equations. Unsteady experiment with constant velocity field  $U = 0.05$ , finite-time evolution with final time  $T = 1$ , and initialization with a sinusoidal wave. The  $x$ -axis represents the number of mesh points with a logarithmic scale and the  $y$ -axis is graduated with the base-2 logarithm of the error. The microscopic moments are initialized with the equilibrium values.

We recall the asymptotic expansion of nonconserved moments for a lattice Boltzmann scheme through the general expression (8):

$$Y = \Phi(W) + S^{-1} (\Delta t \Psi_1(W) + \Delta t^2 \Psi_2(W)) + O(\Delta t^3).$$

For the advective D1Q3 scheme with a cosine advection field,

$$Y = \begin{pmatrix} j \\ e \end{pmatrix}, \quad \Phi(\rho) = \begin{pmatrix} \lambda U \cos(kx) \rho \\ \lambda^2 \alpha \rho \end{pmatrix}, \quad \Psi_1 = \beta_1 \rho, \quad \beta_1 = \lambda^2 \begin{pmatrix} u \partial_u - \frac{\alpha+2}{3} \partial_x \\ \lambda (\alpha - 1) \partial_u \end{pmatrix}$$

and

$$\Psi_2 = \beta_2 \rho, \quad \beta_2 = \lambda^3 \begin{pmatrix} 2 \sigma \frac{u}{\lambda} \partial_u^2 - \left( \frac{\alpha+2}{3} \sigma + \frac{\alpha-1}{3} \sigma' \right) \partial_x \partial_u - \frac{\alpha+2}{3} \sigma \frac{u}{\lambda} \partial_x^2 \\ \lambda (\alpha - 1) \left( (\sigma + \sigma') \partial_u^2 - \frac{\alpha+2}{3} \sigma \partial_x^2 \right) \end{pmatrix}.$$

For initialization at order 0, the relation (28) is simply applied. The initialization suggested by Mei, Luo, Lallemand and d'Humières [39] at order 1 is:

$$(29) \quad Y_1(t=0) = \Phi(\rho_0) + \Delta t S^{-1} \beta_1 \rho_0.$$

In the following, we also consider a second-order initialization:

$$(30) \quad Y_2(t=0) = \Phi(\rho_0) + S^{-1} (\Delta t \beta_1 \rho_0 + \Delta t^2 \beta_2 \rho_0).$$

We remark that this framework can certainly be revisited with the new version of lattice Boltzmann schemes through multistep finite difference schemes, as proposed by Bellotti, Graille and Massot [4]. The results of our simulations are presented in the next section.

## 8) Unsteady fields for a constant or variable advective velocity

We first study the uniform advection case. Then we specify the case of cubic parameters. Then we look to nonuniform cosine advection. In all cases, the choice of the initialization



scheme has a great influence on the final precision. Observe also that only one mode is needed for the Fourier approximation when the advecting velocity is constant.

mesh points \ equation order	1	2	3	4
initialization order	0	0	0	0
64	$2.798 \cdot 10^{-3}$	$7.606 \cdot 10^{-4}$	$7.604 \cdot 10^{-4}$	$7.596 \cdot 10^{-4}$
128	$1.218 \cdot 10^{-3}$	$1.983 \cdot 10^{-4}$	$1.983 \cdot 10^{-4}$	$1.982 \cdot 10^{-4}$
256	$5.598 \cdot 10^{-4}$	$4.979 \cdot 10^{-5}$	$4.979 \cdot 10^{-5}$	$4.978 \cdot 10^{-5}$
512	$2.675 \cdot 10^{-4}$	$1.245 \cdot 10^{-5}$	$1.245 \cdot 10^{-5}$	$1.245 \cdot 10^{-5}$
1024	$1.307 \cdot 10^{-4}$	$3.113 \cdot 10^{-6}$	$3.112 \cdot 10^{-6}$	$3.112 \cdot 10^{-6}$
convergence order	1.10	1.99	1.99	1.99

Table 1: Errors measured with the maximum norm between the D1Q3 lattice Boltzmann scheme [with parameters  $\alpha = -1$ ,  $\sigma \equiv \frac{1}{s} - \frac{1}{2} = 0.01$ ,  $s' = 1.2$ ] and various equivalent partial differential equations for an unsteady experiment: constant velocity field  $U = 0.05$ , finite time evolution with final time  $T = 1$ , and initialization with a sinusoidal wave. The error remains second-order accurate even if we use the third-order or the fourth-order equivalent equation for the approximation of the lattice Boltzmann scheme. Figure 5 is an other representation of these results.

With the first-order initialization (29), the results are presented in Figure 6 and Table 2. They become consistent for the three first levels of approximation, but there is no convergence at fourth-order accuracy.

With the second-order initialization (30), the results are displayed in Figure 7 and Table 3. The experimental order of approximation is now coherent up to fourth order. In Table 4, economical initialization orders are used to present an optimal convergence accuracy.

mesh points \ equation order	1	2	3	4
initialization order	1	1	1	1
64	$2.039 \cdot 10^{-3}$	$7.967 \cdot 10^{-6}$	$2.911 \cdot 10^{-6}$	$2.652 \cdot 10^{-6}$
128	$1.020 \cdot 10^{-3}$	$1.648 \cdot 10^{-6}$	$3.544 \cdot 10^{-7}$	$3.290 \cdot 10^{-7}$
256	$5.101 \cdot 10^{-4}$	$3.697 \cdot 10^{-7}$	$4.305 \cdot 10^{-8}$	$4.049 \cdot 10^{-8}$
512	$2.551 \cdot 10^{-4}$	$8.730 \cdot 10^{-8}$	$5.296 \cdot 10^{-9}$	$5.018 \cdot 10^{-9}$
1024	$1.275 \cdot 10^{-4}$	$2.120 \cdot 10^{-8}$	$6.569 \cdot 10^{-10}$	$6.247 \cdot 10^{-10}$
convergence order	1.00	2.13	3.03	3.01

Table 2: Same numerical experiment as the one described in Table 1, except that the initialization has been changed to the first-order approximation (29). The precision is improved for second order and we obtain the third order correctly, but the fourth-order approximation is only converging up to third order.

## NUMERICAL APPROXIMATIONS OF A LATTICE BOLTZMANN SCHEME

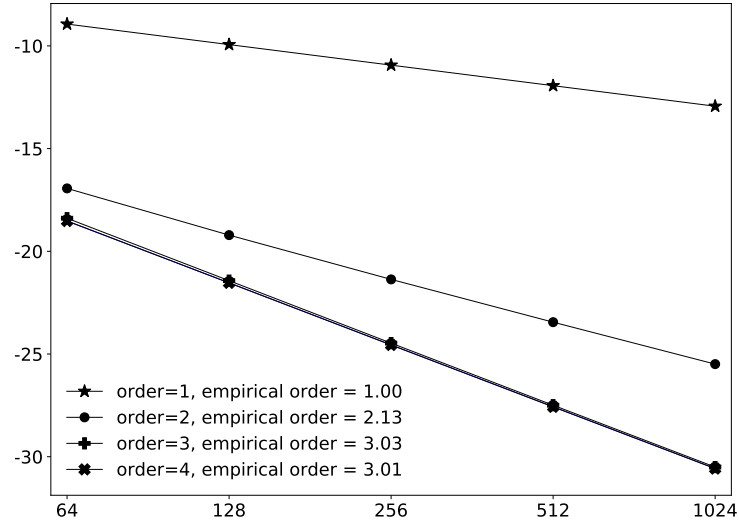


Figure 6: Same experiment as the one described in Figure 5 with the initialization of the microscopic moments at first order following (29).

mesh points \ equation order	1	2	3	4
initialization order	2	2	2	2
64	$2.039 \cdot 10^{-3}$	$5.607 \cdot 10^{-6}$	$1.397 \cdot 10^{-6}$	$6.191 \cdot 10^{-7}$
128	$1.020 \cdot 10^{-3}$	$1.332 \cdot 10^{-6}$	$1.382 \cdot 10^{-7}$	$3.997 \cdot 10^{-8}$
256	$5.101 \cdot 10^{-4}$	$3.299 \cdot 10^{-7}$	$1.485 \cdot 10^{-8}$	$2.506 \cdot 10^{-9}$
512	$2.551 \cdot 10^{-4}$	$8.233 \cdot 10^{-8}$	$1.703 \cdot 10^{-9}$	$1.567 \cdot 10^{-10}$
1024	$1.275 \cdot 10^{-4}$	$2.057 \cdot 10^{-8}$	$2.034 \cdot 10^{-10}$	$9.798 \cdot 10^{-12}$
convergence order	1.00	2.02	3.18	3.99

Table 3: Same numerical experiment as the one described in Table 1, except that the initialization has been changed to the second-order approximation (30). The precision order is now consistent with the approximation order.

mesh points \ equation order	1	2	3	4
initialization order	0	0	1	2
64	$2.798 \cdot 10^{-3}$	$7.606 \cdot 10^{-4}$	$2.911 \cdot 10^{-6}$	$6.191 \cdot 10^{-7}$
128	$1.218 \cdot 10^{-3}$	$1.983 \cdot 10^{-4}$	$3.544 \cdot 10^{-7}$	$3.997 \cdot 10^{-8}$
256	$5.598 \cdot 10^{-4}$	$4.979 \cdot 10^{-5}$	$4.305 \cdot 10^{-8}$	$2.506 \cdot 10^{-9}$
512	$2.675 \cdot 10^{-4}$	$1.245 \cdot 10^{-5}$	$5.296 \cdot 10^{-9}$	$1.567 \cdot 10^{-10}$
1024	$1.307 \cdot 10^{-4}$	$3.113 \cdot 10^{-6}$	$6.569 \cdot 10^{-10}$	$9.798 \cdot 10^{-12}$
convergence order	1.10	1.99	3.03	3.99

Table 4: Optimal initialization orders for the numerical experiment described in Table 1. The precision order is now consistent with the approximation order without any extra calculation for the initialization at the lowest orders.

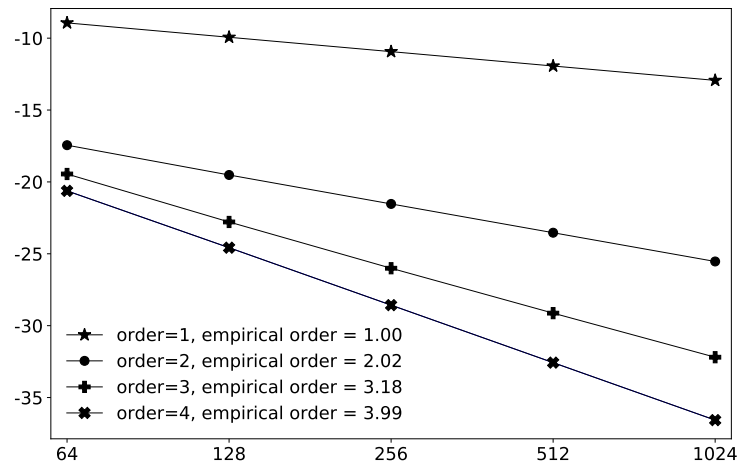


Figure 7: Same experiment as the one described in Figure 5, with the initialization of the microscopic moments at second order following (30).

In a second series of experiments with a constant velocity field, we use cubic parameters:

$$U = 0.05, \alpha = -1, \sigma = 0.01,$$

as previously. The second relaxation coefficient  $s'$  such that the relation (23) is satisfied:

$$(31) \quad \sigma' = 0.072425, \quad s' = 1.7469537493994847$$

with  $\sigma' \equiv \frac{1}{s'} - \frac{1}{2}$ . The initial condition is still a sine wave and we need only one term in the Fourier series.

In Table 5, the initialization for the second-order approximation is only of order zero and the cubic convergence property is not obtained. On the other hand, when the initialization for the second-order partial differential equation is first order accurate (see Table 6), the second-order and third-order approximations are identical.

mesh points \ equation order	1	2	3	4
initialization order	0	0	1	2
64	$2.826 \cdot 10^{-3}$	$7.882 \cdot 10^{-4}$	$2.181 \cdot 10^{-6}$	$6.455 \cdot 10^{-7}$
128	$1.219 \cdot 10^{-3}$	$1.988 \cdot 10^{-4}$	$2.332 \cdot 10^{-7}$	$4.063 \cdot 10^{-8}$
256	$5.598 \cdot 10^{-4}$	$4.980 \cdot 10^{-5}$	$2.665 \cdot 10^{-8}$	$2.544 \cdot 10^{-9}$
512	$2.675 \cdot 10^{-4}$	$1.245 \cdot 10^{-5}$	$3.174 \cdot 10^{-9}$	$1.590 \cdot 10^{-10}$
1024	$1.307 \cdot 10^{-4}$	$3.113 \cdot 10^{-6}$	$3.869 \cdot 10^{-10}$	$9.951 \cdot 10^{-12}$
convergence order	1.11	2.00	3.11	4.00

Table 5: Errors measured with the maximum norm between the D1Q3 lattice Boltzmann scheme with cubic parameter (31) for  $\alpha = -1$ ,  $\sigma \equiv \frac{1}{s} - \frac{1}{2} = 0.01$ . Even if the relaxation parameters have been fitted in order to obtain third-order accuracy with the second-order equivalent partial differential equation, the error remains second-order accurate in this case.

## NUMERICAL APPROXIMATIONS OF A LATTICE BOLTZMANN SCHEME

mesh points \ equation order	1	2	3	4
initialization order	0	1	1	2
64	$2.826 \cdot 10^{-3}$	$2.181 \cdot 10^{-6}$	$2.181 \cdot 10^{-6}$	$6.455 \cdot 10^{-7}$
128	$1.219 \cdot 10^{-3}$	$2.332 \cdot 10^{-7}$	$2.332 \cdot 10^{-7}$	$4.063 \cdot 10^{-8}$
256	$5.598 \cdot 10^{-4}$	$2.665 \cdot 10^{-8}$	$2.665 \cdot 10^{-8}$	$2.544 \cdot 10^{-9}$
512	$2.675 \cdot 10^{-4}$	$3.174 \cdot 10^{-9}$	$3.174 \cdot 10^{-9}$	$1.590 \cdot 10^{-10}$
1024	$1.307 \cdot 10^{-4}$	$3.869 \cdot 10^{-10}$	$3.869 \cdot 10^{-10}$	$9.951 \cdot 10^{-12}$
convergence order	1.11	3.11	3.11	4.00

Table 6: Same numerical experiment as the one described in Table 5, except that the initialization scheme is first-order accurate when comparing with the second-order equivalent partial differential equation. The third-order terms of the partial differential equation are identically null in this case due to the choice of a set of cubic parameters, and the order of accuracy jumps to third order.

When the velocity is no longer constant but given by the relation (1), the modes are coupled as detailed in Section 5. We have used 30 active modes in the Fourier series. In Tables 7 to 9, we experiment with the three types of initialization, (28), (29) and (30). The results are qualitatively identical to the previous experiments with a uniform vector field. When the initialization is done with the equilibrium (28), the lattice Boltzmann scheme can be compared with equivalent partial differential equations only at second order, as detailed in Table 7. For the first order (29), third-order accuracy can be obtained. Nevertheless, the fourth-order differential model is only third-order accurate (Table 8). With a second-order initialization (30), the asymptotic partial differential equation of a given degree is an approximation of the lattice Boltzmann scheme with the same degree, as presented in Table 9.

mesh points \ equation order	1	2	3	4
initialization order	0	0	0	0
64	$5.625 \cdot 10^{-3}$	$1.172 \cdot 10^{-3}$	$1.120 \cdot 10^{-3}$	$1.088 \cdot 10^{-3}$
128	$2.534 \cdot 10^{-3}$	$2.952 \cdot 10^{-4}$	$2.819 \cdot 10^{-4}$	$2.778 \cdot 10^{-4}$
256	$1.195 \cdot 10^{-3}$	$7.327 \cdot 10^{-5}$	$6.992 \cdot 10^{-5}$	$6.940 \cdot 10^{-5}$
512	$5.793 \cdot 10^{-4}$	$1.823 \cdot 10^{-5}$	$1.739 \cdot 10^{-5}$	$1.733 \cdot 10^{-5}$
1024	$2.851 \cdot 10^{-4}$	$4.547 \cdot 10^{-6}$	$4.337 \cdot 10^{-6}$	$4.329 \cdot 10^{-6}$
convergence order	1.07	2.00	2.00	2.00

Table 7: Same numerical experiment as the one described in Table 1; the uniform vector field is replaced by a cosine velocity (1) with  $U_0 = 0.05$ . As in the previous experiment, the error remains second-order accurate even if we use the third-order or the fourth-order equivalent equation for the approximation of the lattice Boltzmann scheme.

mesh points \ equation order	1	2	3	4
initialization order	1	1	1	1
64	$4.561 \cdot 10^{-3}$	$1.087 \cdot 10^{-4}$	$5.628 \cdot 10^{-5}$	$2.446 \cdot 10^{-5}$
128	$2.259 \cdot 10^{-3}$	$1.982 \cdot 10^{-5}$	$6.495 \cdot 10^{-6}$	$2.427 \cdot 10^{-6}$
256	$1.126 \cdot 10^{-3}$	$4.124 \cdot 10^{-6}$	$7.747 \cdot 10^{-7}$	$2.622 \cdot 10^{-7}$
512	$5.620 \cdot 10^{-4}$	$9.336 \cdot 10^{-7}$	$9.441 \cdot 10^{-8}$	$3.018 \cdot 10^{-8}$
1024	$2.808 \cdot 10^{-4}$	$2.216 \cdot 10^{-7}$	$1.165 \cdot 10^{-8}$	$3.610 \cdot 10^{-9}$
convergence order	1.01	2.23	3.06	3.18

Table 8: Same numerical experiment as the one described in Table 7. The initialization is now given by the first-order approximation (29). The precision is improved for the second-order partial differential equation and we obtain the third-order correctly. But the fourth-order approximation is converging only up to third order.

mesh points \ equation order	1	2	3	4
initialization order	2	2	2	2
64	$4.548 \cdot 10^{-3}$	$9.505 \cdot 10^{-5}$	$4.264 \cdot 10^{-5}$	$1.082 \cdot 10^{-5}$
128	$2.257 \cdot 10^{-3}$	$1.807 \cdot 10^{-5}$	$4.742 \cdot 10^{-6}$	$6.741 \cdot 10^{-7}$
256	$1.125 \cdot 10^{-3}$	$3.904 \cdot 10^{-6}$	$5.540 \cdot 10^{-7}$	$4.162 \cdot 10^{-8}$
512	$5.620 \cdot 10^{-4}$	$9.060 \cdot 10^{-7}$	$6.678 \cdot 10^{-8}$	$2.544 \cdot 10^{-9}$
1024	$2.808 \cdot 10^{-4}$	$2.182 \cdot 10^{-7}$	$8.191 \cdot 10^{-9}$	$1.522 \cdot 10^{-10}$
convergence order	1.00	2.19	3.08	4.03

Table 9: Same numerical experiment as the one described in Table 7. The initialization is now given by the second order approximation (30). The precision order is now consistent with the approximation order.

Optimal initialization orders for the numerical experiment with sinusoidal velocity can be made precise as follows:

$$\left\{ \begin{array}{ll} \text{partial differential equation order} = 1 \text{ or } 2 : & \text{initialization at order } 0 \\ \text{partial differential equation order} = 3 : & \text{initialization at order } 1 \\ \text{partial differential equation order} = 4 : & \text{initialization at order } 2. \end{array} \right.$$

The precision order is now consistent with the approximation order without any extra calculation for the initialization at the lowest orders.

If the initial condition is no longer a sinusoidal wave but a constant state, the results presented in Tables 7 to 9 are essentially unchanged. We present in Table 10 the analogue of Table 5 for this case.

mesh points \ equation order	1	2	3	4
initialization order	0	0	1	2
64	$6.050 \cdot 10^{-4}$	$3.597 \cdot 10^{-5}$	$1.224 \cdot 10^{-5}$	$1.306 \cdot 10^{-6}$
128	$2.932 \cdot 10^{-4}$	$7.528 \cdot 10^{-6}$	$1.475 \cdot 10^{-6}$	$8.102 \cdot 10^{-8}$
256	$1.447 \cdot 10^{-4}$	$1.699 \cdot 10^{-6}$	$1.800 \cdot 10^{-7}$	$5.034 \cdot 10^{-9}$
512	$7.194 \cdot 10^{-5}$	$4.024 \cdot 10^{-7}$	$2.221 \cdot 10^{-8}$	$3.130 \cdot 10^{-10}$
1024	$3.587 \cdot 10^{-5}$	$9.784 \cdot 10^{-8}$	$2.758 \cdot 10^{-9}$	$1.943 \cdot 10^{-11}$
convergence order	1.02	2.13	3.03	4.01

Table 10: Optimal initialization orders for the numerical experiment with sinusoidal velocity described in Table 7. The initial condition is changed from a sinusoidal function to a constant state. Each asymptotic partial differential equation presents a precision order consistent with its approximation order.

We tried also to apply a cubic choice of coefficients for the non homogeneous case. We have not observed any spectacular improved precision. There is no inconsistency because the cubic parameters have been explicated with the hypothesis of a constant velocity field.

## 9) Long-time asymptotic study

It is always difficult to reconcile an expansion of a regular solution when the solution is steady. For instance, in steady forced Poiseuille flow the body force must balance the viscous stress. However, the body force typically appears at leading order, while the viscous stress arises at first order relative to the spatial step. Then within the acoustic scaling framework, we obtain different stationary solutions for different meshes as the number of mesh points increases. We refer, *e.g.*, to the contribution [22] for Poiseuille flow with anti-bounce-back boundary conditions.

In this section, we first present the numerical analysis of the spectral properties of the D1Q3 scheme. Then we derive a simple numerical method to achieve a stationary solution at second order. Finally the spectral approach developed in the previous sections is adapted to this stationary case. We report the results of the numerical simulations. We conclude with a preliminary analysis of our analytical and numerical results.

We put in evidence some intrinsic properties of the D1Q3 lattice Boltzmann scheme with the first unstationary mode. One step of the algorithm on a grid with  $N$  mesh points can be written

$$(32) \quad f(t + \Delta t) = A_{D1Q3} f(t)$$

with  $A_{D1Q3}$  the global iteration matrix of order  $3N \times 3N$  of this linear scheme. The matrix  $A_{D1Q3}$  contains all information relative to collision and advection for all the vertices. With an Arnoldi algorithm (see *e.g.* [35]), we extract the first eigenmode of the matrix  $A_{D1Q3}$ . This eigenvalue  $\gamma$  is numerically real in our case and we introduce a scaled parameter  $\Gamma$  defined as follows. From the operator  $\alpha_2$  in (18), we first introduce the discrete equivalent

diffusivity  $\kappa = \lambda \Delta x \sigma^{\frac{\alpha+2}{3}}$ . Then for a simulation with a wave number  $k$ , we set

$$(33) \quad \Gamma = -\frac{\gamma}{\kappa k^2}$$

and the minus sign is introduced for positive numbers. With this definition of  $\Gamma$ , the diffusion equation leads to a numerical value of  $\Gamma$  equal some integer. This is the scaled first eigenvalue of the iteration matrix  $A_{D1Q3}$ . Then from the corresponding eigenvector  $f_\gamma$ , we extract the conserved moment

$$(34) \quad \rho_\gamma = \sum_{j=1}^{j=3} f_{\gamma,j}.$$

It is a function defined at all mesh points. We have represented in Figures 8 to 11 the corresponding modes for  $U = 0, 0.0005, 0.005$  and  $0.05$ .

The very interesting observation concerns the evolution of the eigenvalue  $\Gamma$  as function of velocity and number of mesh points ( $N = 64, 128, 356, 512$ ) presented in Figure 12. A spectacular growth occurs for the largest velocity. In practice, the lattice Boltzmann scheme is much more viscous than proposed by the natural scaling  $\kappa k^2$ . We have also observed that for large values of the velocity  $U$ , we find values for  $\Gamma$  roughly proportional to  $UN$ .

We have done numerical experiments with three advective velocities given by the relation (1) with  $U = 0.0005$ ,  $U = 0.005$  and  $U = 0.05$ . For each of these parameters, we have used four discretizations with 64, 128, 256 and 512 mesh points. We have made various choices for the approximation of the D1Q3 stationary field.

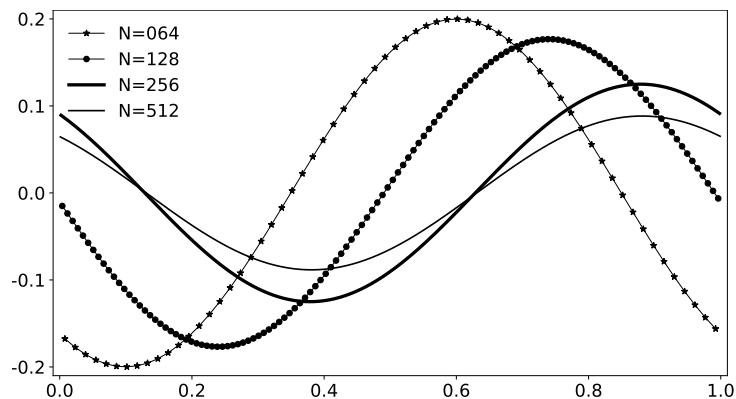


Figure 8: First eigenmode of the stationary D1Q3 discrete dynamics,  $U = 0$ . We have  $\Gamma_{64} = 1.00053560$ ,  $\Gamma_{128} = 1.00013382$ ,  $\Gamma_{256} = 1.00003341$  and  $\Gamma_{512} = 1.00000831$ . The difference between  $\Gamma$  and its integer part is due to rounding errors.

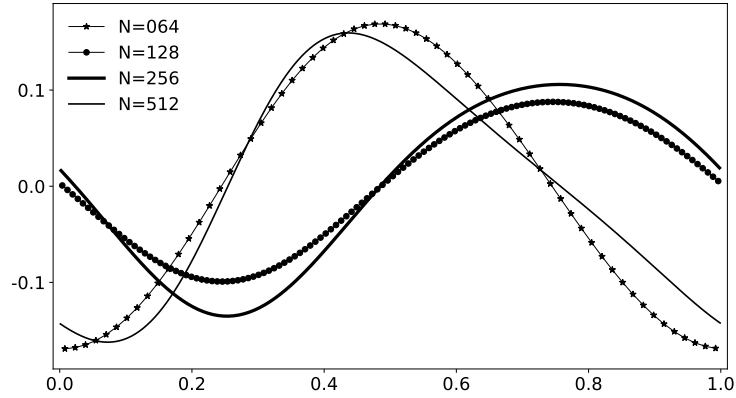


Figure 9: First eigenmode of the stationary D1Q3 discrete dynamics,  $U = 0.0005$ . We have  $\Gamma_{64} = 1.00193081$ ,  $\Gamma_{128} = 1.00572981$ ,  $\Gamma_{256} = 1.02241778$  and  $\Gamma_{512} = 1.08930892$ .

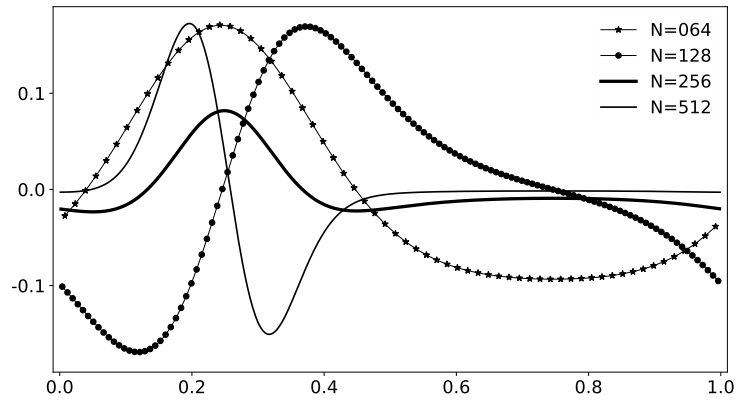


Figure 10: First eigenmode of the stationary D1Q3 discrete dynamics,  $U = 0.005$ . We have  $\Gamma_{64} = 1.13928618$ ,  $\Gamma_{128} = 1.54649116$ ,  $\Gamma_{256} = 3.00825658$  and  $\Gamma_{512} = 6.75648764$ .

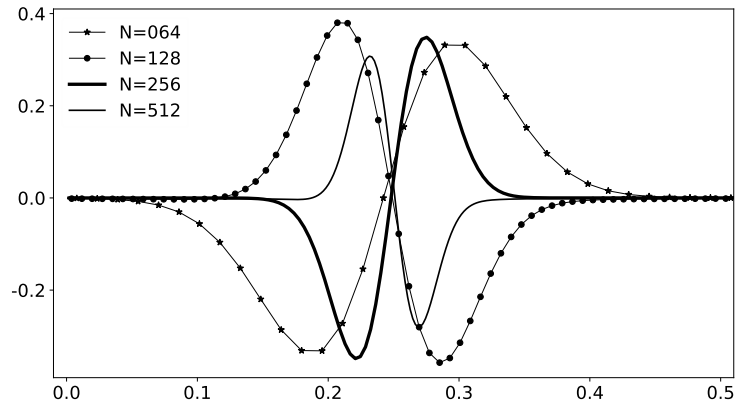


Figure 11: First eigenmode of the stationary D1Q3 discrete dynamics,  $U = 0.05$ . We have  $\Gamma_{64} = 8.62260312$ ,  $\Gamma_{128} = 17.81972445$ ,  $\Gamma_{256} = 36.16622885$  and  $\Gamma_{512} = 72.84095421$ .



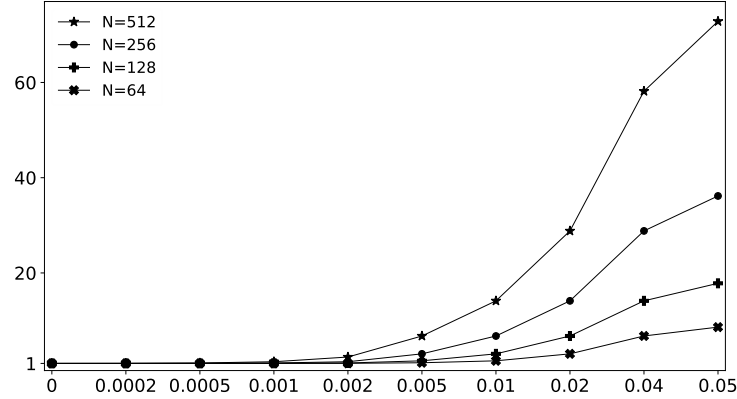


Figure 12: First eigenvalue  $\Gamma$  defined in (33) for the stationary D1Q3 discrete dynamics as a function of velocity and number of mesh points. Observe that the  $x$ -scale is neither linear nor logarithmic to clearly highlight the numerical values.

When we study the equivalent partial differential equation of the lattice Boltzmann scheme, we remark that the equation

$$\partial_t \rho + \partial_x (\lambda U \cos(kx) \rho) - \mu \partial_x^2 \rho = 0$$

is a simple approximation at second-order accuracy. Moreover, we observe that the analytical expression of the stationary solution for the equation with the integral condition

$$(35) \quad \int_0^L \rho(x) dx = 1.$$

can be made explicit as

$$(36) \quad \rho(x) = K \exp\left(\frac{\lambda U}{k \mu} \sin(kx)\right).$$

The normalization constant  $K$  in relation (36) is chosen such that the condition (35) is satisfied.

We then compare the numerical solution obtained with the D1Q3 scheme with the numerical solution of Fourier series truncated with 30 active modes. We introduce an operator  $A$  obtained at various orders from the relation (26) typically and

$$A_\infty = \frac{1}{\partial_x} A.$$

Then  $A_\infty \rho = \text{constant}$  and this constant is zero by periodicity of all the functions of the problem. Then  $A_\infty \rho = 0$  with an operator  $A_\infty$  given at various orders by

$$A_\infty^1 = \lambda m_u - \mu \partial_x$$

at order 1,

$$A_\infty^2 = A_\infty^1 + \mu m_u \partial_x m_u$$

at order 2 and

$$A_\infty^3 = A_\infty^2 + \xi_u m_u \partial_x m_u \partial_x m_u + \xi_{xu} \partial_x^2 m_u + \xi_{ux} m_u \partial_x^2$$

at order 3 and finally,

$$\left\{ \begin{array}{l} A_\infty^4 = A_\infty^3 + \zeta_{u4} m_u \partial_x m_u \partial_x m_u \partial_x m_u + \zeta_{xxuu} \partial_x^2 m_u \partial_x m_u + \zeta_{uxxu} m_u \partial_x^3 m_u \\ \quad + \zeta_{uuxx} m_u \partial_x m_u \partial_x^2 + \zeta_{x4} \partial_x^3 \end{array} \right.$$

at order 4.

For  $U = 0.0005$ , The parameters of the D1Q3 scheme are identical to those chosen for unstationary simulations [ $\alpha = -1$ ,  $s = 1.5$ ,  $s' = 1.2$ ] and we again use 30 Fourier modes. the quantitative results are presented in Table 11. With  $s' = 1.5$  the convergence results are very similar to the ones of Table 11.

mesh points \ equation order	1	2	3	4
64	$8.182 \cdot 10^{-5}$	$8.167 \cdot 10^{-5}$	$5.455 \cdot 10^{-5}$	$6.935 \cdot 10^{-8}$
128	$4.495 \cdot 10^{-5}$	$4.483 \cdot 10^{-5}$	$2.997 \cdot 10^{-5}$	$1.113 \cdot 10^{-8}$
256	$2.616 \cdot 10^{-5}$	$2.611 \cdot 10^{-5}$	$1.744 \cdot 10^{-5}$	$2.067 \cdot 10^{-9}$
512	$1.601 \cdot 10^{-5}$	$1.610 \cdot 10^{-5}$	$1.068 \cdot 10^{-5}$	$4.836 \cdot 10^{-10}$
convergence order	0.78	0.78	0.78	2.39

Table 11: Differences between the lattice Boltzmann D1Q3 scheme and various equivalent equations for a stationary experiment with  $U = 0.0005$ .

mesh points \ equation order	1	2	3	4
64	$1.362 \cdot 10^{-3}$	$1.378 \cdot 10^{-3}$	$9.083 \cdot 10^{-4}$	$2.886 \cdot 10^{-6}$
128	$8.538 \cdot 10^{-4}$	$8.845 \cdot 10^{-4}$	$5.692 \cdot 10^{-4}$	$8.780 \cdot 10^{-7}$
256	$6.183 \cdot 10^{-4}$	$6.437 \cdot 10^{-4}$	$4.122 \cdot 10^{-4}$	$3.066 \cdot 10^{-7}$
512	$4.578 \cdot 10^{-4}$	$4.750 \cdot 10^{-4}$	$3.052 \cdot 10^{-4}$	$1.052 \cdot 10^{-7}$
convergence order	0.52	0.51	0.52	1.58

Table 12: Differences between the lattice Boltzmann D1Q3 scheme and various equivalent equations for a stationary experiment with  $U = 0.005$ .

mesh points \ equation order	1	2	3	4
64	$3.883 \cdot 10^{-2}$	$4.042 \cdot 10^{-2}$	$2.590 \cdot 10^{-2}$	$6.585 \cdot 10^{-4}$
128	$2.856 \cdot 10^{-2}$	$2.967 \cdot 10^{-2}$	$1.904 \cdot 10^{-2}$	$2.439 \cdot 10^{-4}$
256	$2.057 \cdot 10^{-2}$	$2.136 \cdot 10^{-2}$	$1.372 \cdot 10^{-2}$	$8.820 \cdot 10^{-5}$
512	$1.468 \cdot 10^{-2}$	$1.523 \cdot 10^{-2}$	$9.790 \cdot 10^{-3}$	$3.153 \cdot 10^{-5}$
convergence order	0.47	0.47	0.47	1.46

Table 13: Differences between the lattice Boltzmann D1Q3 scheme and various equivalent equations for a stationary experiment with  $U = 0.05$ .

We observe that increasing the order of accuracy increases the quality of the approximation between the lattice Boltzmann scheme and the computation with Fourier series. We observe that it takes very many timesteps before the solution approaches its large-time limit to sufficient accuracy. This is consistent with the relaxation diffusion time  $\tau = \frac{\lambda}{\mu \Delta x k^2}$  measured with our scaling. For example, with 512 mesh points, we have used more than

3,400,000 time steps to reach the numerical result presented in Table 13. This difficulty in reaching the stationary state is directly correlated with the high value of the eigenvalue (72.8) in this case. We observe also that the stationary solution given by the asymptotic expansion is globally correct with errors between  $10^{-5}$  and  $10^{-10}$ . The convergence order is, however, slower than expected with the order of the partial differential equation. Nevertheless, the convergence order for the formal fourth-order approximation (fourth column of Table 11) is 2.39.

For  $U = 0.005$ , we present the numerical results in Figures 13 and 14 and the quantitative residuals in Table 12. The parameters of the D1Q3 scheme are identical to those chosen for the other simulations. The convergence process when the mesh is refined is slow. We have, for example, for the fourth-order partial differential equation (fourth column in Table 12), that a least-square fitting gives a convergence order of 1.58.

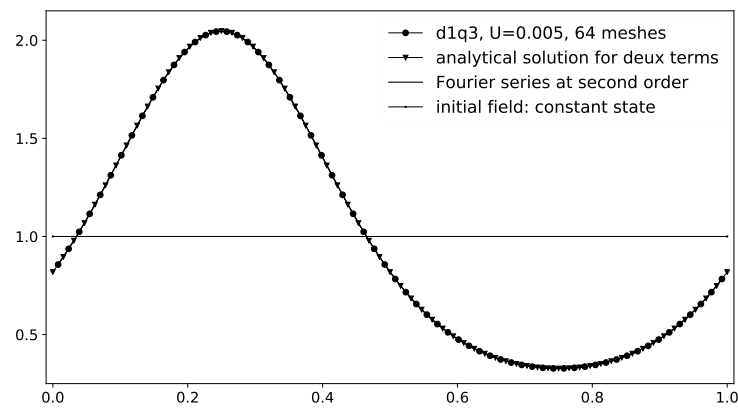


Figure 13: Stationary field for a sinusoidal advection field with  $U = 0.005$  and 64 mesh points. The analytic formula (36) obtained with the advective terms and only the uniform dissipation gives a very correct approximation of the stationary asymptotic solution obtained with the D1Q3 lattice Boltzmann scheme. It is just necessary to compute precisely the constant  $K$  in order to satisfy the integral condition (35).

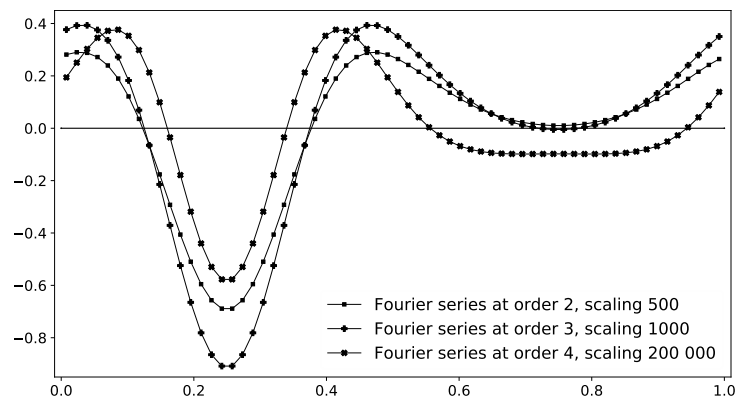


Figure 14: Stationary field,  $U = 0.005$ , 64 mesh points. Errors obtained for various levels of approximation.

When  $U = 0.05$ , we use 30 Fourier modes for 64 and 128 mesh points and 60 modes with 256 and 512 mesh points. The results are presented in Table 13. As advection speed increases, convergence also becomes increasingly difficult. Nevertheless, the speed of convergence towards the stationary state is not directly correlated with the order of the underlying partial differential equation. For example, the numerical order of convergence for the fourth-order partial differential equation is only 1.46.

We have no complete explanation for the low orders of convergence reported in Tables 11 to 13. Observe that the complete discrete dynamics (32) is diverging, as reported in Figure 12, whereas the conserved moment defined as usual by (34) is converging towards some given function as the number of iterations tends to infinity. Nevertheless, in studies of the finite difference method, it is well known (see *e.g.* [36]) that the truncation error  $\theta_{\Delta t}$  is not identical to the error  $\varepsilon_{\Delta t}$ . We have in general for a global time  $T = N\Delta t$  composed of  $N$  iterations,

$$\varepsilon_{\Delta t} \leq C(T) \theta_{\Delta t}.$$

When the global integration time  $T$  is fixed (see Sections 6 to 8), we have a classical stability problem and the error and the truncation errors have the same order of convergence. This kind of analysis can probably be extended for the high-order asymptotic expansion studied in this contribution.

When simulation time tends towards infinity, the discrete dynamical system (32) can diverge exponentially as shown in Figure 12. In particular, some eigenmodes of the pure stationary lattice Boltzmann scheme correspond to an unstable dynamics. Nevertheless, the conserved quantity defined in (34) is converging towards a constant state. The choice of this moment plays the role of a filter inside a diverging process. As a result, the error analysis is difficult in the stationary case. We can reasonably assume that the error  $\varepsilon_{\Delta t}$  and the truncation error  $\theta_{\Delta t}$  behave as  $\varepsilon_{\Delta t} \simeq C(T) \theta_{\Delta t}$ . Moreover, the coefficient  $C(T)$  is in general tending towards infinity as  $T$  tends to infinity. This kind of discrete stability violating the continuous stability criterion has been reported in the analysis of spectral methods (see *e.g.* [7]). Then the convergence accuracy is the result of the confrontation of a diverging stability coefficient and a converging truncation error. These remarks are not completely satisfactory. Nevertheless they offer the beginnings of an explanation for the curious convergence of stationary fields compared to the convergence results for a finite-time evolution.

## 10) Conclusion

In this contribution, we have extended the ABCD asymptotic analysis developed in [18] and [19] to a inhomogeneous linear problem. It has been necessary to develop a library of Fourier series to approximate with high accuracy the equivalent partial differential equations at orders 1 to 4. The differential operators have been explicated with the help of formal calculation and, in particular, the Sagemath [44] library.

We have proven by numerical experiment that the asymptotic equivalent partial differential equations constitute a good approximation of the D1Q3 lattice Boltzmann scheme. A major surprise in our study concerns the finite-time evolution. We have put in evidence the importance of a correct initialization order to force the Boltzmann scheme to simulate a partial

differential equation at high-order and obtain a convergence order consistent with the formal approximation order.

For a stationary problem after a long time evolution, we put in evidence that pure stationary modes of the lattice Boltzmann scheme can be unstable with a sinusoidal advective velocity. Nevertheless, the asymptotic expansion conducts to more and more precise approximations as the size of the mesh tends to zero. The models suggested by the partial differential equations are asymptotically correct but the order of accuracy is not the one suggested by the order of the partial differential equation. We leave this question to be addressed in a future work.

It would be also useful to consider a two-dimensional situation to get information about anisotropic defects of lattice Boltzmann schemes.

## Acknowledgments

This work has been supported by a public grant from the Fondation Mathématique Jacques Hadamard as part of the “Investissement d’avenir” project, reference ANR-11-LABX-0056-LMH, LabEx LMH. FD thanks Thomas Bellotti for an enlightening conversation on the order of initialization of a multistep scheme. FD thanks also the Beijing Computational Science Research Center and in particular Li-Shi Luo for their hospitality during the summer 2023. Last but not least, the referees proposed excellent suggestions that were not present in our initial text. These have been included in the final version of this work.

## Annex A. Proof of Proposition 3

We first recall the general result presented in [18] and [19]. We have

$$(37) \quad \left\{ \begin{array}{l} \Gamma_1(W) = A W + B \Phi(W) \\ \Psi_1(W) = d\Phi(W).\Gamma_1(W) - (C W + D \Phi(W)) \\ \Gamma_2(W) = B \Sigma \Psi_1(W) \\ \Psi_2(W) = \Sigma d\Psi_1(W).\Gamma_1(W) + d\Phi(W).\Gamma_2(W) - D \Sigma \Psi_1(W) \\ \Gamma_3(W) = B \Sigma \Psi_2(W) + \frac{1}{12} B_2 \Psi_1(W) - \frac{1}{6} B d\Psi_1(W).\Gamma_1(W) \\ \Psi_3(W) = \Sigma d\Psi_1(W).\Gamma_2(W) + d\Phi(W).\Gamma_3(W) - D \Sigma \Psi_2(W) + \Sigma d\Psi_2(W).\Gamma_1(W) \\ \quad + \frac{1}{6} D d\Psi_1(W).\Gamma_1(W) - \frac{1}{12} D_2 \Psi_1(W) - \frac{1}{12} d(d\Psi_1(W).\Gamma_1(W)).\Gamma_1(W) \\ \Gamma_4(W) = B \Sigma \Psi_3(W) + \frac{1}{4} B_2 \Psi_2(W) + \frac{1}{6} B D_2 \Sigma \Psi_1(W) - \frac{1}{6} A B \Psi_2(W) \\ \quad - \frac{1}{6} B d(d\Phi.\Gamma_1).\Gamma_2(W) - \frac{1}{6} B d(d\Phi.\Gamma_2).\Gamma_1(W) \\ \quad - \frac{1}{6} B \Sigma d(d\Psi_1(W).\Gamma_1).\Gamma_1(W). \end{array} \right.$$

With the one-dimensional relations (11), we have in particular

$$B \Phi = \bar{B} \partial_x \Phi = \bar{B} \partial_x (E(x) W) = \bar{B} \delta W.$$

Then  $\Gamma_1 = \bar{A} \partial_x W + \bar{B} \delta W = \alpha_1 W$  with  $\alpha_1 = \bar{A} \partial_x + \bar{B} \delta$  and the first relation of the family (14) is proven. We have as previously  $D \Phi = \bar{D} \partial_x (E(x) W) = \bar{D} \delta W$  and  $\Psi_1(W) = d\Phi(W).\Gamma_1(W) - (C W + D \Phi(W)) = E \alpha_1 W - (\bar{C} \partial_x W + \bar{D} \delta W) = [E \alpha_1 - (\bar{C} \partial_x + \bar{D} \delta)] W \equiv \beta_1 W.$

Then the second relation in (14) relative to  $\beta_1$  is established.

From the fact that the matrix  $\Sigma$  is constant, we have now

$$\Gamma_2(W) = B \Sigma \Psi_1(W) = \bar{B} \partial_x \Sigma \beta_1 W = \bar{B} \Sigma \partial_x \beta_1 W \equiv \alpha_2 W$$

and the relation in (14) relative to  $\alpha_2$  is proven.

When we differentiate the vector field  $\Psi_1(W)$ , we have  $d\Psi_1(W).\xi = \beta_1 \xi$  and  $d\Psi_1(W).\Gamma_1(W) = \beta_1 \alpha_1 W$ . Then

$$\begin{aligned} \Psi_2(W) &= \Sigma d\Psi_1(W).\Gamma_1(W) + d\Phi(W).\Gamma_2(W) - D \Sigma \Psi_1(W) \\ &= \Sigma \beta_1 \alpha_1 W + E \alpha_2 W - \bar{D} \delta_x \Sigma \beta_1 W = (\Sigma \beta_1 \alpha_1 + E \alpha_2 - \bar{D} \Sigma \partial_x \beta_1) W \equiv \beta_2 W \end{aligned}$$

and the relation relative to  $\beta_2$  in (14) is proven. We have also

$$B_2 = (AB + BD) = \bar{A} \partial_x \bar{B} \partial_x + \bar{B} \partial_x \bar{D} \partial_x = (\bar{A} \bar{B} + \bar{B} \bar{D}) \partial_x^2 = \bar{B}_2 \partial_x^2.$$

In consequence,

$$\begin{aligned} \Gamma_3(W) &= B \Sigma \Psi_2(W) + \frac{1}{12} B_2 \Psi_1(W) - \frac{1}{6} B d\Psi_1(W).\Gamma_1(W) \\ &= \bar{B} \Sigma \partial_x \beta_2 W + \frac{1}{12} \bar{B}_2 \partial_x^2 \beta_1 W - \frac{1}{6} \bar{B} \partial_x \beta_1 \alpha_1 W \\ &= (\bar{B} \Sigma \partial_x \beta_2 + \frac{1}{12} \bar{B}_2 \partial_x^2 \beta_1 - \frac{1}{6} \bar{B} \partial_x \beta_1 \alpha_1) W \equiv \alpha_3 W \end{aligned}$$

and the expression of the operator  $\alpha_3$  in (14) is established. From the relation (37), we have  $d(d\Psi_1(W).\Gamma_1(W)).\xi = d(\beta_1 \alpha_1 W).\xi$  and

$d(d\Psi_1(W).\Gamma_1(W)).\Gamma_1(W) = \beta_1 \alpha_1 \alpha_1 W = \beta_1 \alpha_1^2 W$ . Then

$$\begin{aligned} \Psi_3(W) &= \Sigma d\Psi_1(W).\Gamma_2(W) + d\Phi(W).\Gamma_3(W) - D \Sigma \Psi_2(W) + \Sigma d\Psi_2(W).\Gamma_1(W) \\ &\quad + \frac{1}{6} D d\Psi_1(W).\Gamma_1(W) - \frac{1}{12} D_2 \Psi_1(W) - \frac{1}{12} d(d\Psi_1(W).\Gamma_1(W)).\Gamma_1(W) \\ &= \Sigma \beta_1 \alpha_2 W + E \alpha_3 W - \bar{D} \partial_x \Sigma \beta_2 W + \Sigma \beta_2 \alpha_1 W \\ &\quad + \frac{1}{6} \bar{D} \partial_x \beta_1 \alpha_1 W - \frac{1}{12} \bar{D}_2 \partial_x^2 \beta_1 W - \frac{1}{12} \beta_1 \alpha_1^2 W \\ &= (\Sigma \beta_1 \alpha_2 + E \alpha_3 - \bar{D} \partial_x \Sigma \beta_2 + \Sigma \beta_2 \alpha_1 + \frac{1}{6} \bar{D} \partial_x \beta_1 \alpha_1 - \frac{1}{12} \bar{D}_2 \partial_x^2 \beta_1 - \frac{1}{12} \beta_1 \alpha_1^2) W \end{aligned}$$

and the relation (14) concerning  $\beta_3$  is established.

We observe now that

$$B d(d\Phi.\Gamma_2).\xi = \bar{B} \partial_x d(E \alpha_2 W).\xi = \bar{B} \delta \alpha_2 \xi \quad \text{and} \quad B d(d\Phi.\Gamma_2).\Gamma_1(W) = \bar{B} \delta \alpha_2 \alpha_1 W.$$

We have finally

$$\begin{aligned} \Gamma_4(W) &= B \Sigma \Psi_3(W) + \frac{1}{4} B_2 \Psi_2(W) + \frac{1}{6} B D_2 \Sigma \Psi_1(W) - \frac{1}{6} A B \Psi_2(W) \\ &\quad - \frac{1}{6} B d(d\Phi.\Gamma_1).\Gamma_2(W) - \frac{1}{6} B d(d\Phi.\Gamma_2).\Gamma_1(W) - \frac{1}{6} B \Sigma d(d\Psi_1(W).\Gamma_1).\Gamma_1(W) \\ &= \bar{B} \Sigma \partial_x \beta_3 W + \frac{1}{4} \bar{B}_2 \partial_x^2 \beta_2 W + \frac{1}{6} \bar{B} \bar{D}_2 \Sigma \partial_x^3 \beta_1 W - \frac{1}{6} \bar{A} \bar{B} \partial_x^2 \beta_2 W \\ &\quad - \frac{1}{6} \bar{B} \delta \alpha_1 \alpha_2 W - \frac{1}{6} \bar{B} \delta \alpha_2 \alpha_1 W - \frac{1}{6} \bar{B} \Sigma \partial_x \beta_1 \alpha_1^2 W \\ &= \left[ \bar{B} \Sigma \partial_x \beta_3 + \frac{1}{4} \bar{B}_2 \partial_x^2 \beta_2 + \frac{1}{6} \bar{B} \bar{D}_2 \Sigma \partial_x^3 \beta_1 - \frac{1}{6} \bar{A} \bar{B} \partial_x^2 \beta_2 - \frac{1}{6} \bar{B} \delta \alpha_1 \alpha_2 \right. \\ &\quad \left. - \frac{1}{6} \bar{B} \delta \alpha_2 \alpha_1 - \frac{1}{6} \bar{B} \Sigma \partial_x \beta_1 \alpha_1^2 \right] W \equiv \alpha_4 W \end{aligned}$$

and the last relation of (14) giving the operator  $\alpha_4$  is explicated.  $\square$

## Annex B. Proof of Proposition 4

We start from the relations (14) that we write again which we rewrite for clarity of reading:

$$\left\{ \begin{array}{l} \alpha_1 = \bar{A} \partial_x + \bar{B} \delta \\ \beta_1 = E \alpha_1 - (\bar{C} \partial_x + \bar{D} \delta) \\ \alpha_2 = \bar{B} \Sigma \partial_x \beta_1 \\ \beta_2 = \Sigma \beta_1 \alpha_1 + E \alpha_2 - \bar{D} \Sigma \partial_x \beta_1 \\ \alpha_3 = \bar{B} \Sigma \partial_x \beta_2 + \frac{1}{12} \bar{B}_2 \partial_x^2 \beta_1 - \frac{1}{6} \bar{B} \partial_x \beta_1 \alpha_1 \\ \beta_3 = \Sigma \beta_1 \alpha_2 + E \alpha_3 - \bar{D} \Sigma \partial_x \beta_2 + \Sigma \beta_2 \alpha_1 + \frac{1}{6} \bar{D} \partial_x \beta_1 \alpha_1 - \frac{1}{12} \beta_1 \alpha_1^2 - \frac{1}{12} \bar{D}_2 \partial_x^2 \beta_1 \\ \alpha_4 = \bar{B} \Sigma \partial_x \beta_3 + \frac{1}{4} \bar{B}_2 \partial_x^2 \beta_2 + \frac{1}{6} \bar{B} \bar{D}_2 \Sigma \partial_x^3 \beta_1 - \frac{1}{6} \bar{A} \bar{B} \partial_x^2 \beta_2 \\ \quad - \frac{1}{6} \bar{B} \delta \alpha_1 \alpha_2 - \frac{1}{6} \bar{B} \delta \alpha_2 \alpha_1 - \frac{1}{6} \bar{B} \Sigma \partial_x \beta_1 \alpha_1^2. \end{array} \right.$$

With the D1Q3 lattice Boltzmann scheme, we have

$$\delta = \begin{pmatrix} \lambda \partial_u \\ \lambda^2 \alpha \partial_x \end{pmatrix}, \quad E(x) = \begin{pmatrix} \lambda U \cos(kx) \\ \lambda^2 \alpha \end{pmatrix}, \quad \Sigma = \begin{pmatrix} \sigma & 0 \\ 0 & \sigma' \end{pmatrix}$$

and

$$\bar{A} = 0, \quad \bar{B} = (1, 0), \quad \bar{C} = \begin{pmatrix} \frac{2\lambda^2}{3} \\ 0 \end{pmatrix}, \quad \bar{D} = \begin{pmatrix} 0 & \frac{1}{3} \\ \lambda^2 & 0 \end{pmatrix}.$$

Then we obtain  $\alpha_1 = \delta = \lambda \partial_u$ ,

$$\begin{aligned} \beta_1 &= \begin{pmatrix} u \\ \lambda^2 \alpha \end{pmatrix} \lambda \partial_u - \begin{pmatrix} \frac{2\lambda^2}{3} \\ 0 \end{pmatrix} \partial_x - \begin{pmatrix} 0 & \frac{1}{3} \\ \lambda^2 & 0 \end{pmatrix} \begin{pmatrix} \lambda \partial_u \\ \lambda^2 \alpha \partial_x \end{pmatrix} = \begin{pmatrix} \lambda u \partial_u - \frac{2}{3} \lambda^2 \partial_x - \frac{\lambda^2}{3} \alpha \partial_x \\ \lambda^3 \alpha \partial_u - \lambda^3 \partial_u \end{pmatrix} \\ &= \begin{pmatrix} \lambda u \partial_u - \frac{1}{3} \lambda^2 (\alpha + 2) \partial_x \\ \lambda^3 (\alpha - 1) \partial_u \end{pmatrix} \end{aligned}$$

and the relation (17) is proven. We have for second order accuracy  $\bar{B} \Sigma = (\sigma, 0)$ . Then  $\alpha_2 = \sigma \partial_x [\lambda u \partial_u - \frac{\lambda^2}{3} (\alpha + 2) \partial_x] = \lambda^2 \sigma (\partial_u^2 - \frac{\alpha+2}{3} \partial_x^2)$ .

For the microscopic variables, we have

$$\begin{aligned} \beta_2 &= \begin{pmatrix} \sigma & 0 \\ 0 & \sigma' \end{pmatrix} \lambda^2 \begin{pmatrix} \lambda u \partial_u - \frac{2}{3} \lambda^2 \partial_x - \frac{\lambda^2}{3} \alpha \partial_x \\ \lambda^3 \alpha \partial_u - \lambda^3 \partial_u \end{pmatrix} \lambda \partial_u + \begin{pmatrix} u \\ \lambda^2 \alpha \end{pmatrix} \lambda^2 \sigma (\partial_u^2 - \frac{\alpha+2}{3} \partial_x^2) \\ &\quad - \lambda \begin{pmatrix} 0 & \frac{\sigma'}{3} \\ \lambda^2 \sigma & 0 \end{pmatrix} \begin{pmatrix} u \partial_u - \frac{1}{3} \lambda^2 (\alpha + 2) \partial_x \\ \lambda^2 (\alpha - 1) \partial_u \end{pmatrix}. \end{aligned}$$

For the first component,

$$\begin{aligned} \beta_2^1 &= \sigma (\lambda u \partial_u - \frac{\alpha+2}{3} \lambda^2 \partial_x) \lambda \partial_u + \lambda^2 u \sigma (\partial_u^2 - \frac{\alpha+2}{3} \partial_x^2) - \lambda^3 \frac{\sigma'}{3} \partial_x (\alpha - 1) \partial_u \\ &= 2 \lambda^2 \sigma u \partial_u^2 - \frac{\alpha+2}{3} \lambda^3 \partial_x \partial_u - \lambda^2 \frac{\alpha+2}{3} u \partial_x^2 - \lambda^3 (\alpha - 1) \frac{\sigma'}{3} \partial_x \partial_u \\ &= \lambda^3 [2 \sigma \frac{u}{\lambda} \partial_u^2 - (\frac{\alpha+2}{3} \sigma - \frac{\alpha-1}{3} \sigma') \partial_x \partial_u - \frac{\alpha+2}{3} \sigma \frac{u}{\lambda} \partial_x^2] \end{aligned}$$

and for the second component

$$\begin{aligned} \beta_2^2 &= \lambda^2 \sigma' (\lambda (\alpha - 1) \partial_u) \lambda \partial_u + \lambda^4 \alpha \sigma (\partial_u^2 - \frac{\alpha+2}{3} \partial_x^2) - \lambda^4 \sigma (\frac{u}{\lambda} \partial_u - \frac{\alpha+2}{3} \partial_x) \\ &= \lambda^4 [(\alpha - 1) \sigma' \partial_u^2 + \alpha \sigma (\partial_u^2 - \frac{\alpha+2}{3} \partial_x^2) - \sigma (\partial_u^2 - \frac{\alpha+2}{3} \partial_x^2)] \\ &= \lambda^4 (\alpha - 1) ((\sigma + \sigma') \partial_u^2 - \frac{\alpha+2}{3} \sigma \partial_x^2). \end{aligned}$$

Then the relations (18) are established. At third order, we have from (14),

$$\alpha_3 = \bar{B} \Sigma \partial_x \beta_2 + \frac{1}{12} \bar{B}_2 \partial_x^2 \beta_1 - \frac{1}{6} \bar{B} \partial_x \beta_1 \alpha_1$$

$$\begin{aligned}
 &= \sigma \partial_x \beta_2^1 + \frac{1}{12} (0, \frac{1}{3}) \partial_x \beta_1 - \frac{1}{6} \bar{B} \partial_x \left( \frac{\lambda u \partial_u - \frac{2}{3} \lambda^2 \partial_x - \frac{\lambda^2}{3} \alpha \partial_x}{\lambda^3 \alpha \partial_u - \lambda^3 \partial_u} \right) \lambda \partial_u \\
 &= \lambda^3 \sigma \partial_x \left[ 2 \sigma \frac{u}{\lambda} \partial_u^2 - \left( \frac{\alpha+2}{3} \sigma - \frac{\alpha-1}{3} \sigma' \right) \partial_x \partial_u - \frac{\alpha+2}{3} \sigma \frac{u}{\lambda} \partial_x^2 \right] + \frac{1}{12} \frac{\lambda^3}{3} (\alpha - 1) \partial_x^2 \partial_u \\
 &\quad - \frac{\lambda}{6} \partial_x \left[ \lambda u \partial_u - \frac{\alpha+2}{3} \lambda^2 \partial_x \right] \lambda \partial_u \\
 &= \lambda^3 \left[ \left( 2 \sigma^2 - \frac{1}{6} \right) \partial_u^3 + \left[ -\sigma \left( \frac{\alpha+2}{3} \sigma + \frac{\alpha-1}{3} \sigma' \right) + \frac{\alpha-1}{36} + \frac{\alpha+2}{18} \right] \partial_x^2 \partial_u - \frac{\alpha+2}{3} \sigma^2 \partial_u \partial_x^2 \right] \\
 &= \lambda^3 \left[ \left( 2 \sigma^2 - \frac{1}{6} \right) \partial_u^3 + \left( \frac{\alpha+2}{3} \left( \frac{1}{6} - \sigma^2 \right) + \frac{\alpha-1}{3} \left( \frac{1}{12} - \sigma \sigma' \right) \right) \partial_x^2 \partial_u - \frac{\alpha+2}{3} \sigma^2 \partial_u \partial_x^2 \right]
 \end{aligned}$$

and the relation (19) is proven. We have now

$$\beta_3 = \Sigma \beta_1 \alpha_2 + E \alpha_3 - \bar{D} \Sigma \partial_x \beta_2 + \Sigma \beta_2 \alpha_1 + \frac{1}{6} \bar{D} \partial_x \beta_1 \alpha_1 - \frac{1}{12} \beta_1 \alpha_1^2 - \frac{1}{12} \bar{D}_2 \partial_x^2 \beta_1$$

and we can precise these seven terms:

$$\begin{aligned}
 \Sigma \beta_1 \alpha_2 &= \begin{pmatrix} \sigma & 0 \\ 0 & \sigma' \end{pmatrix} \lambda \left( \lambda^3 \left[ 2 \sigma \frac{u}{\lambda} \partial_u^2 - \left( \frac{\alpha+2}{3} \sigma - \frac{\alpha-1}{3} \sigma' \right) \partial_x \partial_u - \frac{\alpha+2}{3} \sigma \frac{u}{\lambda} \partial_x^2 \right] \right) \lambda^2 \sigma \left( \partial_u^2 - \frac{\alpha+2}{3} \partial_x^2 \right) \\
 E \alpha_3 &= \begin{pmatrix} u \\ \lambda^2 \alpha \end{pmatrix} \lambda^3 \left[ \left( 2 \sigma^2 - \frac{1}{6} \right) \partial_u^3 + \left( \frac{\alpha+2}{3} \left( \frac{1}{6} - \sigma^2 \right) + \frac{\alpha-1}{3} \left( \frac{1}{12} - \sigma \sigma' \right) \right) \partial_x^2 \partial_u - \frac{\alpha+2}{3} \sigma^2 \partial_u \partial_x^2 \right] \\
 -\bar{D} \Sigma \partial_x \beta_2 &= - \begin{pmatrix} 0 & \frac{1}{3} \\ \lambda^2 & 0 \end{pmatrix} \begin{pmatrix} \sigma & 0 \\ 0 & \sigma' \end{pmatrix} \partial_x \left( \lambda^3 \left[ 2 \sigma \frac{u}{\lambda} \partial_u^2 - \left( \frac{\alpha+2}{3} \sigma - \frac{\alpha-1}{3} \sigma' \right) \partial_x \partial_u - \frac{\alpha+2}{3} \sigma \frac{u}{\lambda} \partial_x^2 \right] \right) \\
 \Sigma \beta_2 \alpha_1 &= \begin{pmatrix} \sigma & 0 \\ 0 & \sigma' \end{pmatrix} \begin{pmatrix} \lambda^3 \left[ 2 \sigma \frac{u}{\lambda} \partial_u^2 - \left( \frac{\alpha+2}{3} \sigma - \frac{\alpha-1}{3} \sigma' \right) \partial_x \partial_u - \frac{\alpha+2}{3} \sigma \frac{u}{\lambda} \partial_x^2 \right] \\ \lambda^4 (\alpha - 1) \left( (\sigma + \sigma') \partial_u^2 - \frac{\alpha+2}{3} \sigma \partial_x^2 \right) \end{pmatrix} \lambda \partial_u \\
 \frac{1}{6} \bar{D} \partial_x \beta_1 \alpha_1 &= \frac{1}{6} \begin{pmatrix} 0 & \frac{1}{3} \\ \lambda^2 & 0 \end{pmatrix} \partial_x \left( \frac{\lambda u \partial_u - \frac{1}{3} \lambda^2 (\alpha + 2) \partial_x}{\lambda^3 (\alpha - 1) \partial_u} \right) \lambda \partial_u \\
 -\frac{1}{12} \beta_1 \alpha_1^2 &= -\frac{1}{12} \begin{pmatrix} \lambda u \partial_u - \frac{1}{3} \lambda^2 (\alpha + 2) \partial_x \\ \lambda^3 (\alpha - 1) \partial_u \end{pmatrix} \lambda^2 \partial_u^2 \\
 -\frac{1}{12} \bar{D}_2 \partial_x^2 \beta_1 &= -\frac{\lambda^2}{12} \begin{pmatrix} 1 & 0 \\ 0 & \frac{1}{3} \end{pmatrix} \partial_x^2 \left( \frac{\lambda u \partial_u - \frac{1}{3} \lambda^2 (\alpha + 2) \partial_x}{\lambda^3 (\alpha - 1) \partial_u} \right).
 \end{aligned}$$

Then the first component of  $\beta_3$  is given by the relation

$$\begin{aligned}
 \beta_3^1 &= \lambda^4 \left[ \frac{\alpha+2}{9} \left[ - (1 - \alpha) \sigma \sigma' + ((\alpha + 2) \sigma^2 + \frac{1}{4}) \right] \partial_x^3 \right. \\
 &\quad + U \left[ - 2 \frac{\alpha+2}{3} \sigma^2 + \frac{1-\alpha}{3} \sigma \sigma' + \frac{1+\alpha}{12} \right] \partial_x^2 \partial_u - 2U \frac{\alpha+2}{3} \sigma^2 \partial_u \partial_x^2 \\
 &\quad \left. + \left[ - 2 \frac{\alpha+2}{3} \sigma^2 + \frac{1-\alpha}{3} (2 \sigma \sigma' + \sigma'^2 - \frac{1}{4}) \right] \partial_x \partial_u^2 + (5 \sigma^2 - \frac{1}{4}) U \partial_u^3 \right]
 \end{aligned}$$

and the second is given by

$$\begin{aligned}
 \beta_3^2 &= \lambda^5 \left[ \frac{1-\alpha}{3} \left[ (\alpha + 2) \sigma^2 + (1 + 2\alpha) \sigma \sigma' - \frac{1+\alpha}{4} \right] \partial_x^2 \partial_u + (1 - \alpha) \frac{\alpha+2}{3} \sigma (\sigma + \sigma') \partial_u \partial_x^2 \right. \\
 &\quad \left. - (1 - \alpha) \left( 2 \sigma^2 + 2 \sigma \sigma' + \sigma'^2 - \frac{1}{4} \right) \partial_u^3 \right].
 \end{aligned}$$

The relation (20) is proven. Finally,

$$\begin{aligned}
 \alpha_4 &= \bar{B} \Sigma \partial_x \beta_3 + \frac{1}{4} \bar{B}_2 \partial_x^2 \beta_2 + \frac{1}{6} \bar{B} \bar{D}_2 \Sigma \partial_x^3 \beta_1 - \frac{1}{6} \bar{A} \bar{B} \partial_x^2 \beta_2 - \frac{1}{6} \bar{B} \delta \alpha_1 \alpha_2 \\
 &\quad - \frac{1}{6} \bar{B} \delta \alpha_2 \alpha_1 - \frac{1}{6} \bar{B} \Sigma \partial_x \beta_1 \alpha_1^2.
 \end{aligned}$$

After some lines of algebra,

$$\frac{1}{\lambda^4} \alpha_4 = \left[ \left( \frac{\alpha+2}{3} \right)^2 \sigma^3 + (\alpha - 1) \frac{\alpha+2}{9} \sigma^2 \sigma' - \frac{\alpha+2}{36} \alpha \sigma \right] \partial_x^4$$



$$\begin{aligned}
& + \left[ -2 \frac{\alpha+2}{3} \sigma^3 + 2 \frac{1-\alpha}{3} \sigma^2 \sigma' + \frac{1-\alpha}{3} \sigma \sigma'^2 + \frac{1+2\alpha}{9} \sigma + \frac{\alpha-1}{12} \sigma' \right] \partial_x^2 \partial_u^2 \\
& + \left[ -2 \frac{\alpha+2}{3} \sigma^3 + \frac{1-\alpha}{3} \sigma^2 \sigma' + \frac{7+5\alpha}{36} \sigma \right] \partial_u \partial_x^2 \partial_u + \frac{\alpha+2}{3} \sigma \left( -2 \sigma + \frac{1}{6} \right) \partial_u^2 \partial_x^2 + \sigma \left( 5 \sigma^2 - \frac{3}{4} \right) \partial_u^4 \\
= & \left[ \frac{\alpha+2}{9} \left( (\alpha+2) \sigma^3 - (1-\alpha) \sigma^2 \sigma' - \frac{\alpha}{4} \sigma \right) \partial_x^4 \right. \\
& + \left. \left[ -2 \frac{\alpha+2}{3} \sigma^3 + \frac{1-\alpha}{3} (2 \sigma^2 \sigma' + \sigma \sigma'^2 - \frac{1}{4} \sigma') + \frac{1+2\alpha}{9} \sigma \right] \partial_x^2 \partial_u^2 \right. \\
& + \left. \left[ -2 \frac{\alpha+2}{3} \sigma^3 + \frac{1-\alpha}{3} \sigma^2 \sigma' + \frac{7+5\alpha}{36} \sigma \right] \partial_u \partial_x^2 \partial_u + \frac{\alpha+2}{3} \sigma \left( -2 \sigma + \frac{1}{6} \right) \partial_u^2 \partial_x^2 + \sigma \left( 5 \sigma^2 - \frac{3}{4} \right) \partial_u^4 \right]
\end{aligned}$$

and the relation (21) is established. This completes the proof.  $\square$

## References

- [1] W. E. Arnoldi, “The principle of minimized iterations in the solution of the matrix eigenvalue problem”, *Quarterly of Applied Mathematics*, volume 9, pages 17–29, 1951.
- [2] A. Augier, F. Dubois, L. Gouarin, B. Graille, “Linear lattice Boltzmann schemes for Acoustic: parameter choices and isotropy properties”, *Computers and Mathematics with Applications*, volume 65, pages 845-863, 2013.
- [3] A. Augier, F. Dubois, B. Graille, P. Lallemand, “On rotational invariance of lattice Boltzmann schemes”, *Computers and Mathematics with Applications*, volume 67, pages 239-255, 2014.
- [4] T. Bellotti, B. Graille, M. Massot, “Finite difference formulation of any lattice Boltzmann scheme”, *Numerische Mathematik*, volume 152, pages 1-40, 2022.
- [5] T. Bellotti, “Truncation errors and modified equations for the lattice Boltzmann method via the corresponding Finite Difference schemes”, *ESAIM: Mathematical Modelling and Numerical Analysis*, volume 57, pages 1225-1255, 2023.
- [6] T. Bellotti, “Initialisation from lattice Boltzmann to multi-step Finite Difference methods: modified equations and discrete observability”, *Journal of Computational Physics*, volume 504, 112871, 2024.
- [7] C. Bernardi, Y. Maday, “Spectral methods”, *Handbook of numerical analysis*, volume 5, pages 209-485, 1989.
- [8] B.M. Boghosian, F. Dubois, B. Graille, P. Lallemand, M. M. Tekitek, “Curious Convergence Properties of Lattice Boltzmann Schemes for Diffusion with Acoustic Scaling”, *Communications in Computational Physics*, volume 23, pages 1263-1278, 2018.
- [9] B.M. Boghosian, F. Dubois, B. Graille, P. Lallemand, M. M. Tekitek, “Unexpected convergence of lattice Boltzmann schemes”, *Computers and Fluids*, volume 172, pages 301-311, 2018.
- [10] B.M. Boghosian, F. Dubois, P. Lallemand, “Numerical approximations of a lattice Boltzmann scheme with a family of partial differential equations”, Preliminary report, arxiv.org-2403.19231, March 2024.
- [11] J. E. Broadwell, “Shock structure in a simple discrete velocity gas”, *Physics of Fluids*, volume 7, pages 1243-1247, 1964.
- [12] S. Chapman, T.G. Cowling, *The mathematical theory of non-uniform gases*, Cambridge University Press, 1939.

- [13] S. Chen, G. D. Doolen, “Lattice Boltzmann Method for Fluid Flows”, *Annual Review of Fluid Mechanics*, volume 30, pages 329-364, 1998.
- [14] S. Dellacherie, “Construction and analysis of lattice Boltzmann methods applied to a 1D convection-diffusion equation”, *Acta Applicandae Mathematica*, volume 131, pages 69-140, 2014.
- [15] P. J. Dellar, “An interpretation and derivation of the lattice Boltzmann method using Strang splitting”, *Computers and Mathematics with Applications*, volume 65, pages 129-141, 2013.
- [16] F. Dubois, “Equivalent partial differential equations of a lattice Boltzmann scheme”, *Computers and Mathematics with Applications*, volume 55, pages 1441-1449, 2008.
- [17] F. Dubois, “Third order equivalent equation of lattice Boltzmann scheme”, *Discrete and Continuous Dynamical Systems, A*, volume 23, pages 221-248, 2009.
- [18] F. Dubois, “Nonlinear fourth-order Taylor expansion of lattice Boltzmann schemes”, *Asymptotic Analysis*, volume 127, pages 297-337, 2022.
- [19] F. Dubois, B.M. Boghosian, P. Lallemand, “General fourth-order Chapman–Enskog expansion of lattice Boltzmann schemes”, *Computers and Fluids*, volume 266, article 106036, 11 pages, 2023.
- [20] F. Dubois, P. Lallemand, “Towards higher order lattice Boltzmann schemes”, *Journal of Statistical Mechanics, Theory and Experiment*, P06006, 2009.
- [21] F. Dubois, P. Lallemand, “Quartic Parameters for Acoustic Applications of Lattice Boltzmann Scheme”, *Computers and Mathematics with Applications*, volume 61, pages 3404-3416, 2011.
- [22] F. Dubois, P. Lallemand, M. Tekitek, “On anti bounce back boundary condition for lattice Boltzmann schemes”, *Computers and Mathematics with Applications*, volume 79, pages 555-575, 2020.
- [23] F. Dubois, P. Lallemand, “On Single Distribution Lattice Boltzmann Schemes for the Approximation of Navier Stokes Equations”, *Communications in Computational Physics*, volume 34, pages 613-671, 2023.
- [24] J. H. Ferziger, M. Perić, R. L. Street *Computational methods for fluid dynamics*, 1996, fourth edition Springer 2019.
- [25] D. Galloway, U. Frisch, “Dynamo action in a family of flows with chaotic streamlines”, *Geophysical and Astrophysical Fluid Dynamics*, volume 36, pages 53-83, 1986.
- [26] R. Gatignol, “The hydrodynamical description for a discrete velocity model of gas”, *Complex systems*, volume 1, pages 709-725, 1987.
- [27] Z. Guo, C. Shu, *Lattice Boltzmann method and its applications in engineering*, World Scientific, 2013.
- [28] X. He, L.-S. Luo, “Theory of the lattice Boltzmann method: from the Boltzmann equation to the lattice Boltzmann equation”, *Physical Review E*, vol. **56**, pages 6811-6817, 1997.
- [29] M. Hénon, “Viscosity of a lattice gas”, *Complex systems*, volume 1, pages 763-789, 1987.

- [30] X. He, X. Shan, G. D. Doolen, “Discrete Boltzmann equation model for nonideal gases”, *Physical Review E*, vol. **57**, pages R13–R16, 1998.
- [31] D. d’Humières, “Generalized lattice-Boltzmann equations”, in *Rarefied Gas Dynamics: Theory and Simulations*, volume 159 of *AIAA Progress in Astronautics and Aeronautics*, pages 450-458, 1992.
- [32] D. d’Humières, I. Ginzburg, M. Krafczyk, P. Lallemand, L.-S. Luo, “Multiple-relaxation-time lattice Boltzmann models in three dimensions”, *Philosophical Transactions of the Royal Society A: Mathematical, Physical and Engineering Sciences*, volume 15, pages 437-451, 2002.
- [33] D. d’Humières, I. Ginzburg, “Viscosity independent numerical errors for Lattice Boltzmann models: From recurrence equations to “magic” collision numbers”, *Computers And Mathematics with Applications*, volume 58, pages 823-840, 2009.
- [34] T. Krüger, H. Kusumaatmaja, A. Kuzmin, O. Shardt, G. Silva, E. M. Viggen, *The Lattice Boltzmann Method: Principles and Practice*, Springer Verlag, 2017
- [35] P. Lallemand, L.-S. Luo, “Theory of the lattice Boltzmann method: dispersion, dissipation, isotropy, galilean invariance, and stability”, *Physical Review E*, volume 61, pages 6546-6562, 2000.
- [36] P. D. Lax, R.D. Richtmyer, “Survey of the stability of linear finite difference equations”, *Communications in Pure and Applied Mathematics*, volume 9, pages 267-293, 1956.
- [37] E. Leriche, P. Lallemand, G. Labrosse, “Stokes eigenmodes in cubic domain: primitive variable and Lattice Boltzmann formulations”, *Applied Numerical Mathematics*, volume 58, pages 935-945, 2008.
- [38] B. Lucquin, O. Pironneau, *Introduction to scientific computing*, Wiley, 1998.
- [39] R. Mei, L.-S. Luo, P. Lallemand, D. d’Humières, “Consistent initial conditions for lattice Boltzmann simulations”, *Computers and Fluids*, volume 35, pages 855-862, 2006.
- [40] J. T. Oden, J. N. Reddy, *An introduction to the mathematical theory of finite elements*, 1976, Dover Publications, 2011.
- [41] H. Otomo, B. M. Boghosian, F. Dubois, “Two complementary lattice-Boltzmann-based analyses for nonlinear systems”, *Physica A*, volume 486, pages 1000-1011, 2017.
- [42] Y. H. Qian, Y. Zhou, “On higher order dynamics in lattice-based models using Chapman-Enskog method”, *Physical Review E*, volume 61, pages 2103-2106, 2000.
- [43] D. H. Rothman, S. Zaleski, *Lattice-gas cellular automata; simple models of complex hydrodynamics*, Cambridge University Press, Aléa-Saclay collection, 1997.
- [44] SageMath, the Sage Mathematics Software System (Version 7.5.1), The Sage Developers, <http://www.sagemath.org>, 2017.
- [45] S. Simonis, M. Haussmann, L. Kronberg, W. Dörfler, M. J. Krause, “Linear and brute force stability of orthogonal moment multiple-relaxation-time lattice Boltzmann methods applied to homogeneous isotropic turbulence”, *Philosophical Transactions of the Royal Society A: Mathematical, Physical and Engineering Sciences*, volume 379, page 20200405, 2021.

- [46] S. Succi, *The lattice Boltzmann equation for fluid dynamics and beyond*, Clarendon Press, 2001
- [47] R. Verberg and A. J. C. Ladd, "Simulation of low-Reynolds-number flow via a time-independent lattice-Boltzmann method", *Physical Review E*, volume 60, pages 3366-3373, 1999.